Universidad Zaragoza
1542

Trabajo Fin de Máster

Real time motion tracking during magnetic resonance imaging

Autor

Carlos Dieste Orús

Supervisor

Lars G. Hanson

Ponente

Emiliano Bernués del Río

Escuela de Ingeniería y Arquitectura

2016

Technical University of Denmark

Carlos Dieste Orús (s150787)

Real time motion tracking during Magnetic Resonance Imaging

Master's Thesis, July 2016

DTU Electrical Engineering
Department of Electrical Engineering

DANISH RESEARCH
CENTRE FOR
MAGNETIC RESONANCE

CARLOS DIESTE ORÚS (S150787)

Real time motion tracking during Magnetic Resonance Imaging

Master's Thesis, July 2016

Supervisors:

Lars G. Hanson, PhD, Associate Professor at DTU Department of Electrical Engineering

Kristoffer Hougaard Madsen, PhD, Associate Professor at DTU Department of Applied Mathematics and Computer Science

Mads Andersen, PhD, DRCMR

DTU - Technical University of Denmark, Kgs. Lyngby - 2016

Real time motion tracking during Magnetic Resonance Imaging

This report was prepared by:
Carlos Dieste Orús (s150787)

Advisors:
Lars G. Hanson, PhD, Associate Professor at DTU Department of Electrical Engineering
Kristoffer Hougaard Madsen, PhD, Associate Professor at DTU Department of Applied Mathematics and Computer Science
Mads Andersen, PhD, DRCMR

DTU Electrical Engineering
Biomedical Engineering
Technical University of Denmark
Elektrovej, Building 326
2800 Kgs. Lyngby
Denmark
Tel: +45 4525 3576

studieadministration@elektro.dtu.dk

Project period: January 2016- July 2016

ECTS: 30

Education: MSc

Field: Electrical Engineering

Class: Public

Remarks: This report is submitted as partial fulfillment of the requirements for graduation in the above education at the Technical University of Denmark.

To Lars, Mads and Kristoffer, who have introduced me
to the fascinating world of MR.
To all my friends who supported me during this crazy year.
Para mis abuelas, Josefina e Isabel.
Por último, para mis padres por el apoyo incondicional
que me habés mostrado estos seis años.

Abstract

Real time motion tracking during magnetic resonance imaging

Patient motion during magnetic resonance imaging (MRI) represents an issue for the accuracy in the diagnosis through this technique, and its effects vary depending on the acquisition method that is used for the imaging. Several solutions to this problem are presented in the literature according to the type of MR scan that is performed. Prospective motion correction involves the update of the MR scanner geometry in real-time according to the patient motion.

In this thesis, this tracking procedure is aimed to be implemented in real-time for the corresponding update of the scanner parameters. The motion parameters are estimated in this thesis using a novel motion tracking technique that uses the artifacts that appear in the EEG signal during an MRI scan while the patient is wearing an EEG hood. These artifacts are mainly caused by the variation of the magnetic field during the MR scan. Since these artifacts depend on the position and orientation of the EEG loops that the wires and electrodes of the EEG system form, a model of the magnetic field variation over time can be obtained previously according to the imaging sequence that is used. This field variation is used to estimate the patient motion during the scan. A slice by slice tracking method based on this principle is presented in this thesis, using the trigger pulses that are generated by the MR scanner to signal each slice in the EEG measurements. Different strategies of using these triggers are tested until a solution that provides the least possible noisy estimation is found.

Since this estimation method introduces some noise in the motion estimation, a filtering process is needed to smooth the result of the estimated motion parameters. The Kalman filter is implemented and tested for this purpose, since it is suited for the real-time estimation of the motion parameters, and at the same time it provides a smoothed version of the input signal.

Contents

List of Figures

List of Tables

Chapter 1

Introduction

In this first chapter the motivation of this project is presented, along with the state of the art of the prospective motion correction in magnetic resonance imaging, focusing on the motion tracking methods that can be used for it. The scope of this project and the outline of this report are described as well in this chapter.

1.1 Motivation

Magnetic resonance imaging (MRI) is a non-invasive and non-ionizing diagnostic technique that uses strong magnetic fields to visualize the structure of the human body. In particular, brain MRI can be used to analyze physiological and functional responses of the brain. For example, magnetic resonance (MR) spectroscopy allows measuring the concentrations of different metabolites that are generated in a specific region of the brain. Through this technique it is possible to study biochemical changes in the brain, which helps the diagnosis of tumors. Functional magnetic resonance imaging (fMRI) is another MR procedure that is used to analyze the regions of the brain in which neural activity varies while some activity is being performed by the patient.

Unlike other image diagnostic techniques, such as ultrasound imaging, X-ray, computed tomography (CT) or positron emission tomography (PET), MRI is very sensitive to patient motion, which generates imaging artifacts such as blurring or signal loss that may prevent an accurate diagnosis. Due to the procedure that is followed to acquire the MR images during a scan, the patient must be completely still during the acquisition of the data. In fMRI, since the analysis of the brain activity needs the acquisition of MR images for a long period of time, it is very difficult for the patient to be motionless for this long period of time.

1.2 State of the art

In order to compensate patient motion, multiple motion correction techniques can be used. Prospective motion correction implicates updating the MR scanner parameters, such as the reference frequency or the field of view (FOV) in real-time during the acquisition. The continuous update of the scanner involves three steps:

- Obtaining of motion data through a certain tracking system.
- Data processing to transform the motion parameters into the scan parameters that should be updated.
- Update of the scanner imaging sequence. The gradients and RF fields are updated to follow the observed motion.

The motion data can be estimated through different tracking techniques. According to [13], there are three types of methods that can be used to obtain the tracking information:

- Navigators are special RF pulses that can be used to track patient motion during the scan. The position of the patient is estimated according to the time between the moment when the pulse is emmitted and the moment when the pulse is received.
- Field detection methods take advantage of the fact that in MRI different points inside the scanner experience different magnetic field strength due to the gradients that are applied. Different active markers that contain miniature receiving coils are used to locate the patient inside the scanner.
- Optical methods require markers to obtain the patient pose through laser systems, bend sensitive optic fibers or cameras.

In [4] a novel technique of prospective motion correction is described. It uses the gradient artifacts that are present in the electroencephalography (EEG) signals. Those artifacts are generated as a consequence of Faraday's Law of induction when a MRI scan is performed while the patient is wearing an EEG hood.

1.3 Scope

The aim of this project is using the principles that are described in [4] to perform a slice by slice motion tracking using the EEG signals that are acquired during an MRI scan to compensate the patient motion in real-time and avoid imaging artifacts that may happen if the patient moves while a volume is being acquired. However, the prospective update of the scanner is not included in this project.

Since the results of the slice by slice motion estimation may contain some noise as a result of the motion estimation, another purpose of this project is performing a real-time filtered prediction of the per-slice estimation by finding a suited filtering algorithm that provides the best results with the real-time limitations.

1.4 Thesis outline

In chapter 2 an introduction to MR physics and imaging is presented to the reader, along with an introduction to EEG artifacts that are caused by gradient switching during combined EEG-fMRI scans and a deeper description of the consequences of patient motion during the scan. Also the principles of the algorithm that is proposed in [4] are presented. After this, in chapter 3 the per-slice motion tracking algorithm is described, and in chapter 4 the filtering solution to the real-time problem is proposed and assessed. Finally, in chapter 5 the topics that are considered by the author of this project as subject of future work are presented, and in chapter 6 the conclusions of the project are summed up.

Chapter 2

Background

In this chapter the background of this project is presented. First, the basic principles of Magnetic Resonance Imaging and the combined acquisition of Electroencephalography signals and functional magnetic resonance imaging are described. Secondly, the consequences of the movement of the patient during a magnetic resonance scan are explained. Finally, the principles of the motion tracking algorithm that is used in this thesis are presented.

2.1 Magnetic Resonance Imaging physics

This introduction to Magnetic Resonance Imaging (MRI) is targeted at readers with minimal knowledge about the subject. It also can be used as a reminder for those readers who have a certain MRI experience.

Most MR imaging systems are based on signals from Hydrogen nuclei since they are included in the human body in a very high proportion as, for example, part of water molecules. Hydrogen nuclei have an intrinsic magnetic field due to the spin that protons have. This magnetic field is very weak, and it points in the direction of the rotating axis of the nuclei. If a static magnetic field B_0 is applied to the hydrogen nuclei, the nuclei are aligned partially, but the joint contribution of the nuclei creates a net magnetization that can be measured by an external coil.

This equilibrium state in which the nuclei rotate with a certain spin can be disturbed if other magnetic field B_1 is applied in an orthogonal direction from the B_0 field. This magnetic field consists in a RF pulse with a frequency equal to the Larmor frequency, and it is able to rotate the magnetization around it through an angle that depends on the strength of the B_1 field and the duration of the RF pulse.

Due to the RF pulse that is applied, the net magnetization created by the nuclei will start to precess around de direction of the B_0 magnetic field with the so-called Larmor frequency, which is proportional to the static field:

$$f_0 = \gamma B_0 \tag{2.1}$$

where γ is the gyromagnetic radio and is equal to 42.576 MHz/T for protons.

After the RF excitation, the net magnetization will return to equilibrium due to the relaxation of its longitudinal and transversal components.

Relaxation of the longitudinal magnetization is due to the interactions between the magnetic fields of the nuclei. T_1 is the time that defines how the longitudinal magnetization returns to the original equilibrium magnetization.

$$M_z(t) = M_z(t=0)\exp(-t/T_1) + M_0(1-\exp(-t/T_1)) \tag{2.2}$$

Relaxation of the transversal component of the magnetization is caused by the diphase of the spins of the nuclei and also by the interactions between the magnetic fields of the nuclei.

T_2 is the time constant that describes the decreasing of the rotating transversal magnetization.

$$M_{xy}(t) = M_{xy}(t=0)\exp(-j\omega_0 t)\exp(-t/T_2) \tag{2.3}$$

In addition to the T_2 relaxation, the transversal magnetization is affected by inhomogeneity in the B_0 magnetic field, since it increases the relaxation rate of the transversal magnetization:

$$1/T_2^* = 1/T_2 + \gamma \Delta B_0 \tag{2.4}$$

where T_2^* is the time parameter that describes relaxation for the transversal component of the magnetization under inhomogeneity, T_2 is the time parameter that describes relaxation for the transversal component of the magnetization without magnetic field inhomogeneity and ΔB_0 is the intra-voxel magnetic field inhomogeneity.

Contrast in MRI is possible because these relaxation times are different for the different tissues and structures in the human body.

2.2 Image formation

When an MR image from a specific slice is acquired, a gradient must be applied along a certain direction, which is called slice selection direction. This gradient produces a variation of the magnetic field that is added to the static B_0 field along the slice selection direction, and therefore it will influence the frequency at which the nuclei in that slice will precess. If the slice selection gradient is set along the z direction, the magnetic field strength B along this direction will be:

$$B = B_0 + G_z z \tag{2.5}$$

Thus, the precession angular frequency ω will also depend on the position in the z direction, according to eq. 2.1:

$$\omega = \omega_0 + 2\pi\gamma G_z z \tag{2.6}$$

If the RF slice selection pulse is emmited with the new Larmor frequency, only the nuclei that are on-resonance with this frequency, which will be located in a specific slice, will be excited. The thickness of the slice depends on the strength of the gradient and the bandwidth of the RF slice excitation pulse.

MR imaging is performed by building each image as a weighted combination of oscillating patterns in every possible direction and with every possible wavelength. Each oscillating pattern is called phase roll, and is created by applying gradients that vary the magnetic field that is oriented along the longitudinal direction B, with a specific strength for a specific time. Those gradients modify the field strength along the transverse direction to the orientation of the B field.

In order to represent each phase roll, a spatial frequency space is defined, which is called the k-space. Each point in the k-space represents a specific phase roll with a specific wavelength and direction, and can be generated by applying gradients along both directions in the slice plane for a certain time:

$$k_x = \gamma \int_0^t G_x(\tau)\mathrm{d}\tau \tag{2.7}$$

$$k_y = \gamma \int_0^t G_y(\tau)\mathrm{d}\tau \tag{2.8}$$

The signal that is received by the receiving coils will depend on the transversal net magnetization over the three dimensions in space, which will depend on the phase roll that has been accumulated over time due to the effect of the gradients:

$$s_r \propto \iiint M_{xy}(\mathbf{r}) e^{-i\int_0^t \Delta\omega(\mathbf{r},\tau)\mathrm{d}\tau}\mathrm{d}\mathbf{r} = \iiint M_{xy}(\mathbf{r}) e^{-i2\pi\gamma\int_0^t \mathbf{G}(\tau)\mathbf{r}\mathrm{d}\tau}\mathrm{d}\mathbf{r} \tag{2.9}$$

The transversal magnetization that will be recorded for a certain slice depends on the slice thickness, since nuclei outside the slice will not be excited. For a certain slice that is centered in $z = z_0$ with a thickness of Δz, the transversal magnetization that is recorded will be the sum of the magnetization inside the slice along the longitudinal direction:

$$m(x, y) = \int_{z_0-\Delta z/2}^{z_0+\Delta z/2} M_{xy}(x, y, z)\mathrm{d}z \tag{2.10}$$

Thus, the signal that is received by the receiving coils will depend on the transversal net magnetization in each point in the slice, but also on the position in k-space:

$$s_r \propto \iint m(x, y)e^{-i2\pi\gamma \int_0^t [xG_x(\tau)+yG_y(\tau)]\mathrm{d}\tau}\mathrm{d}x\mathrm{d}y = \iint m(x, y)e^{-i2\pi[k_x x+k_y y]}\mathrm{d}x\mathrm{d}y \tag{2.11}$$

Thus, the magnetization in each point in the slice can be reconstructed through a 2-D Fourier transform of the measurements in each point in k-space.

To be able to sample in k-space these gradients must change over time to create different phase rolls. This is achieved through different imaging sequences that combine RF pulses with gradient combinations in the transversal direction of the magnetization.

2.3 EEG-fMRI acquisition

The simultaneous recording of electroencephalography (EEG) and functional MRI (fMRI) combines the ability of the EEG to reflect the brain activity with high temporal resolution with the capacity of fMRI to reflect the changes in the demand of oxygenated blood in the human brain with a relatively high spatial resolution.

Functional magnetic resonance imaging is based on the BOLD (Blood Oxygenated Level Dependent) effect, which describes the changes in the concentration of oxygenated blood in the brain after a stimulus. Deoxyhemoglobin is a substance that is present in non-oxygenated blood, and it is able to locally increase the magnetic field in which it is in by one hundredth of it, because of its paramagnetic nature. This change in the magnetic field induces an inhomogeneity in the voxels in which the vessels that contain non-oxygenated blood are located, and therefore a change in the relaxation rate of the transversal component of the magnetization, according to eq. 2.4. Since oxygenated blood is not paramagnetic, the BOLD effect is used to find the brain regions that are activated by certain motor or sensitive stimulus. After acquiring several MR volumes while the subject is perceiving and not perceiving the stimulus, the time series signal for each voxel throughout the acquired volumes is fitted to a model of the response that is expected for a certain timed paradigm. In the acquisition of the data, a fast acquisition sequence such as Echo Planar Imaging (EPI) with T_2^* weighting is used, in order to detect the changing intra-voxel inhomogeneity.

EPI is a fast imaging technique that uses a single excitation for the acquisition of the entire k-space of every slice. After the slice selective excitation, the fast readout of each phase encoding step is performed due to the strong gradients that are applied in both the phase encoding direction and the readout direction.

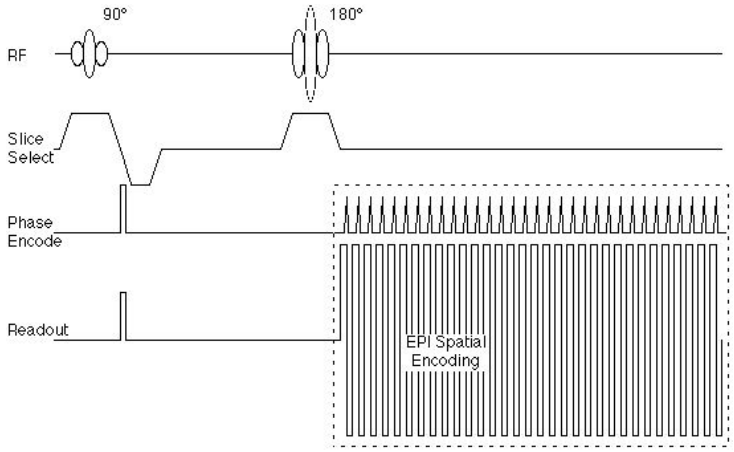

Figure 2.1: *Example of a gradient sequence diagram for the EPI sequence. Figure taken from [7].*

If the subject is wearing an EEG hood during the fMRI scan, those fast-changing magnetic field gradients used for the spatial encoding in the imaging induce an electromotive force in each apparent wire loop (composed the wires and electrodes of the EEG hood) perpendicular to the direction of the varying magnetic field, which is proportional to the variation in the gradients.

As a result, the fast varying gradients induce a very intense electric noise in the measured EEG signal whose amplitude can be up to 100 times larger than the original EEG signal [14] and part of whose frequency components are included in the EEG frequency band (0.5-70 Hz) [3].

For the regular purpose of the combined use of EEG and fMRI, which is monitoring events in the brain with high spatial and temporal resolution than the separate use of EEG or fMRI measurements, those artifacts are removed through different signal processing techniques such as average waveform subtraction [15, 9, 3]. However, since the induced artifacts contain spatial information about the orientation and position of the apparent wire loops, they can also be used to detect motion from the subject during the fMRI acquisition while the patient is wearing an EEG hood.

2.4 Patient motion. Imaging artifacts

For the MR image acquisition, since the gradients must be active during some time during the slice selection phase, but also during the k-space sampling, the acquisition of a whole volume in a MR scan takes some time (between two and three seconds), despite using fast imaging techniques such as EPI, fast Spin-Echo or parallel imaging. During the acquisition of a volume, the subject may move from his or her initial position, distorting the images. Non-voluntary causes such as breathing or twitches can generate this unevitable movement.

Since the two-dimensional Fourier transform defines how the MR images are reconstructed from the measured signal in k-space, it is important to analyze how a physical rotation or translation in the imaging plane would affect the sampling in k-space.

Regarding how the motion affects the sampling if it happens in the imaging plane, a rotation in the image coordinate axis will induce the same rotation in the k-space coordinate axis:

$$m(x\cos\theta + y\sin\theta, -x\sin\theta - y\cos\theta) \leftrightarrow \\ \leftrightarrow s(k_x\cos\theta + k_y\sin\theta, -k_x\sin\theta - k_y\cos\theta) \quad (2.12)$$

where $m(x, y)$ is the transversal magnetization for a certain slice and $s(k_x, k_y)$ is the corresponding 2-D Fourier transform.

On the other side, a translation in the image coordinate axis will cause a change in the phase of the measured signal in k-space that depends on the position in the k-space coordinate axis and the translation in the image coordinate axis:

$$m(x + \Delta x, y + \Delta y) \leftrightarrow s(k_x, k_y)e^{i2\pi[k_x\Delta x + k_y\Delta y]} \quad (2.13)$$

If a rotation in the imaging plane occurs while a certain slice is being acquired, it is possible that not every line in k-space is rotated in the same angle, leading to non-homogeneity in the k-space sampling and possibly to violations in the Nyquist sampling theorem. This is specially relevant in multi-shot sequences, but not in single-shot sequences, such as EPI, since the k-space acquisition for each slice is considered fast enough to be insensitive to in-plane motion. However, since the subject head is a rigid body, if one slice in the head of the subject moves, the rest of the slices will move with the same motion. This motion affects the relative orientation of the subject respect to the scanner coordinate system, and therefore it affects the imaging in following slices as well.

Another relevant type of motion for single-shot sequences is through-plane motion. It takes place in a perpendicular direction to the slice plane, and may lead to either loss of data or to spin-history effects. The first of them happens if some voxels inside a non-excited slice are displaced due to motion to the slice that is being acquired. This type of effects can be corrected by updating the scanner coordinate axis to modify the direction of the gradients for the acquisition of the next slice or volume. Spin-history artifacts provoke that tissues from slices with different excitation history, and therefore different saturation levels, contribute to the signal for a particular slice. This could lead to local changes in the image contrast or unwanted signal fluctuations over time in the time series of EPI volumes that are acquired during an fMRI scan. Since the brain activations in fMRI are estimated from the time series signal of each voxel, these signal fluctuations over time will prevent a reliable statistical analysis of the brain activations. This effect can be avoided by performing an interleaved slice acquisition, which will lead to signal loss, since some non-excited voxels will be moved to the slice that is being acquired. This signal loss is easier to compensate than spin-history artifacts.

Slice acquisition ordering

To avoid imaging artifacts caused by crosstalk between slices due to the thickness of the slice profile or spin history artifacts caused by through-slice motion, in multi-slice MR imaging the slices are usually acquired in a different order than the one in which they are visualized, which usually is ascending order. The most common acquisition orders in which the slices are acquired are ascending, first odd then even, and interleaved.

- In ascending order, the slices are acquired in the same order as they are visualized $(1, 2, 3...)$. An example of ascending order acquisition for coronal slices is shown in figure 2.2. Coronal plane is the acquisition plane for the slices from the human subject data that are acquired using the EPI sequence that is used in this project to test the programmed algorithms, which is described in section 3.2.2.
- Regarding first odd then even acquisition order, the odd numbered slices in the visualizing order are acquired first, and after this, the acquisition of the even numbered slices begins $(1, 3, 5, ..., 2, 4, 6...)$.
- Interleaved acquisition order is usually used to avoid spin-history artifacts. According to this slice acquisition order, the slices are acquired with a certain slice separation, which depends on the number of slices of the acquired volume. This slice separation is defined as:

$$Separation = \left\lfloor \sqrt{N_{slices}} \right\rfloor \tag{2.14}$$

  where N_{slices} is the number of the slices of the acquired volume. Usually, this amount is 42, so the slice separation in the acquisition order is 6. In this case, the acquisition order would be: $1, 7, 13, ..., 31, 37, 2, 8, 14....$

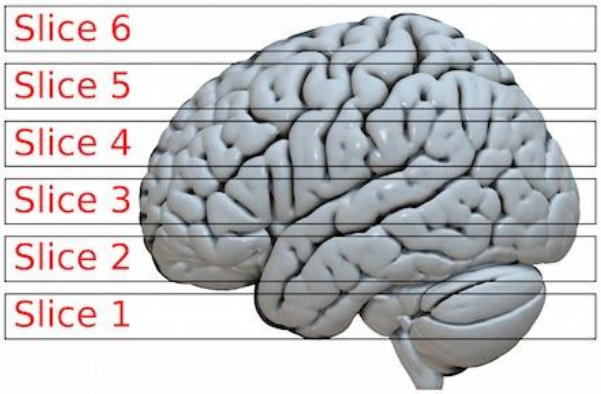

Figure 2.2: *Diagram of the slice visualizing order for coronal slices. Figure taken from [16].*

2.5 Use of an EEG hood for prospective motion correction

In [4] a prospective motion correction technique for MRI using EEG equipment, which is based on signals from gradient switching in an EEG hood, was described.

This prospective motion correction method uses the artifacts that appear in the EEG measurements as a consequence of the switching of the gradients that are used in a certain MR imaging sequence. Those artifacts vary according to the position and orientation of the wire loops that form the EEG electrodes, so it is possible to find out the position and orientation of the subject from the artifacts that are present in the EEG signals that are measured during the acquisition of an MR volume. The electrodes that are part of each wire loop are connected to each other either through the subject scalp or directly by attaching them in pairs. After the motion parameters are calculated, the scanner geometry can be updated to compensate the motion of the subject during the acquisition of the previous volume.

As it is stated before, the magnetic field variation over time that is generated by gradient switching while a volume is being acquired induces an electromotive force in each apparent wire loop perpendicular to the direction of the varying magnetic field, which is proportional to the variation in the gradients in the three directions in space. The voltage that is measured as a consequence of this electromotive force in one of the EEG channels is:

$$\tilde{V}_i(t) = w_{ix}\frac{\partial \tilde{G}_x(t)}{\partial t} + w_{iy}\frac{\partial \tilde{G}_y(t)}{\partial t} + w_{iz}\frac{\partial \tilde{G}_z(t)}{\partial t} \tag{2.15}$$

where $\frac{\partial \tilde{G}_x(t)}{\partial t}, \frac{\partial \tilde{G}_y(t)}{\partial t}, \frac{\partial \tilde{G}_z(t)}{\partial t}$ are linearly filtered versions of $\frac{\partial G_x(t)}{\partial t}, \frac{\partial G_y(t)}{\partial t}, \frac{\partial G_z(t)}{\partial t}$ due to the filtering process that is performed by the EEG system due to the anti-aliasing filters that are necessary because of the limited sampling rate of the measuring system. The weights w_{ix}, w_{iy}, w_{iz} depend on the geometry, position and orientation of the electrode wire loops.

Since the EEG hood electrodes are attached to the subject head, it is considered that the geometry of the wire loops and the relative position between the subject head and the wire loops remain constant during the scan. Therefore, the weights w_{ix}, w_{iy}, w_{iz} can be described in terms of the position and orientation of the subject head.

Due to the fact that the geometry of the head coil is fitted to the geometry of a regular subject head, the subject motion will be small. For those small changes, the relationship between the changes in the position and orientation of the head from a reference position (Δr_h) and the changes in the weights due to that motion (Δw) can be approximated as linear:

$$\Delta w = A \Delta r_h \tag{2.16}$$

where A is a 3Nx6 (N EEG channels) matrix that contains the partial derivatives of the weights with respect to head position parameters, evaluated in the reference position.

The A matrix can be estimated using data from a training scan, where the subject moves stepwise between the acquisition of each volume. The 3D MR images are aligned to obtain the translation and rotation parameters (Δr_h) from a reference position that is defined by the first acquired volume. The weights (Δw) for every EEG channel are calculated by performing a regression between a model of the gradient variation $\frac{\partial \tilde{G}_x(t)}{\partial t}, \frac{\partial \tilde{G}_y(t)}{\partial t}, \frac{\partial \tilde{G}_z(t)}{\partial t}$ and the measured EEG signal for that channel during the scan, according to eq. 2.15. The weights (Δw) can be computed for each volume after the volume has been acquired and the EEG signal for the entire volume is available. After that, the motion parameters are calculated using the calibration matrix, from 2.16.

After this, the scanner field of view can be changed according to the estimated motion parameters by changing the reference frequency of the scanner (translation in k-space) and rotating the gradient waveforms (rotation in k-space). For this reason, the gradient waveform models $\frac{\partial \tilde{G}_x(t)}{\partial t}, \frac{\partial \tilde{G}_y(t)}{\partial t}, \frac{\partial \tilde{G}_z(t)}{\partial t}$ must be updated as well, to maintain the correspondence between the measured gradient artifacts and the scanner gradient waveforms. In [4], the gradient waveform models $\frac{\partial \tilde{G}_x(t)}{\partial t}, \frac{\partial \tilde{G}_y(t)}{\partial t}, \frac{\partial \tilde{G}_z(t)}{\partial t}$ are estimated from a previous scan in which the same sequence is used, during three runs. In each run, only one gradient in one direction is active (G_x, G_y, G_z). From the normalized EEG signals for every channel that are acquired in each run, the first component of the singular value decomposition is taken as the gradient waveform model.

The image alignment

During the calibration process, the acquired time series of fMRI images are aligned to find the relative position of each volume with respect to the first volume, which is established as a zero-motion reference. The realignment is performed through the SPM (Statistical Parametric Mapping) software. SPM [8] is usually used to identify specific brain responses by first performing a pre-processing of the images that involves a motion compensation procedure to counteract the motion of the patient during the scan and a process that registers the fMRI images to a normalized human brain template to help group research. After the pre-processing is performed, SPM performs a regression of the time series signal for each voxel in the fMRI volumes to a general linear model that includes the expected time series response of the brain according to the BOLD effect, which depends on the timed paradigm that has been used during the scan.

SPM is implemented as a Matlab toolbox and can be used either through a graphic user interface (GUI) or by calling the different functions that are included in the toolbox. To find the motion of each volume, the SPM function that performs the realignment returns one set of six relative motion parameters (three translation t_x, t_y, t_z and three rotation r_x, r_y, r_z parameters) for each volume. These motion parameters are used to build the A matrix using eq. 2.16.

Chapter 3

Per-slice motion estimation

In this chapter a per-slice motion estimation method based on the principles of the motion estimation that are described in section 2.5 is presented. The main issues that have been faced during the implementation and how they have been solved, along with the results that have been obtained are described and discussed in this chapter.

3.1 Introduction

In [4] a method for estimating the motion of the subject during an fMRI scan while the subject is wearing an EEG hood is proposed and tested. This method uses the EEG signals that are recorded during the scan to perform a regression to the gradient waveform models for the whole volume for the three directions in space ($\frac{\partial \tilde{G}_x(t)}{\partial t}$, $\frac{\partial \tilde{G}_y(t)}{\partial t}$, $\frac{\partial \tilde{G}_z(t)}{\partial t}$). These models are built from the data that are acquired in a previous scan during three runs, in which only a gradient in each direction is active during each run, respectively.

In section 2.4 it is mentioned that through-plane motion that causes the shift of voxels from non-excited slices to the slice that is being acquired leads to signal loss in the acquired slice. In addition to the signal loss due to through-plane motion, in-plane motion distorts the phase and the magnitude of the k-space data in each slice.

In this chapter, a modification of the algorithm that is described in [4] for the per-volume motion estimation is proposed and tested. The estimation of the subject motion is performed independently for each slice in the volume, enabling a more frequent updating of the scanner parameters during the scan. Thus, the effect of the in-plane motion and the through-plane motion can be compensated in a shorter period of time after they happen if the MR scanner is updated for the acquisition of each slice.

3.2 Methodology

3.2.1 From per-volume to per-slice motion estimation

In order to adapt the per-volume motion estimation that is presented in [4], to perform a per-slice motion estimation, first it is necessary to modify the regression process that estimates the weights from the target EEG signal and the gradient waveform models.

The gradient waveform models

For the modeling of the gradient waveforms, the Singular Value Decomposition (SVD) is performed only using the EEG channels that provide the best estimation of the gradient waveforms. SVD analysis is selected over a weighted averaging of the channels since a model of the gradient waveforms that is robust against noise or non-gradient related artifacts is wanted. In figure 3.4 a comparison between the gradient models that result from the estimation by taking the first component of the SVD analysis (subfigure 3.4(a)) and averaing over the channels that are used (subfigure 3.4(b)) is shown. For this comparison, the human subject data that are described in subsection 3.2.2 was used, and 31 channels are taken for the SVD analysis and the averaging. In figure 3.4 it can be seen that the gradient model estimation for the same fragment of signal is more stable if the first component of the SVD is used than if the averaging over channels is performed.

For the estimation of each gradient waveform, an iterative process that first calculates the SVD and then calculates the mean square error (MSE) between the first principal component of the SVD and the signal from each channel. The channel with the highest MSE is assumed to have the most noise content, and therefor is discarded. The waveforms are normalized to their variance before the MSE is calculated.

In order to find out the amount of channels that should be used in the gradient waveform estimation, an analysis of the combined mean square error for all the channels that contribute to the calculation of the first principal component of the SVD when different amount of channels is performed. The results are displayed in figure 3.5, and show that for the calculation of the three gradient waveform models, the accumulated mean square error decreases as the number of EEG channels that are used decreases, and it decreases with a slope that is fairly constant, except for some discontinuities. This constant slope could indicate that the channels contribute equally to the error, and the discontinuities could indicate that when a key channel is removed from the set of channels that is used for the estimation, the error increases. For this reason, the iterative process that discards the noisiest channel is repeated until the discontinuity in the combined mean square error for all the channels that contribute to the calculation of the gradient model is found.

Figure 3.1 shows how the gradient model estimation is performed for one of the iterations of the algorithm. After the first component of the SVD is calculated, the channel that has the highest mean square error to the first principal component of the SVD is discarded. The algorithm also looks for discontinuities in the accumulated MSE for the channels in each iteration.

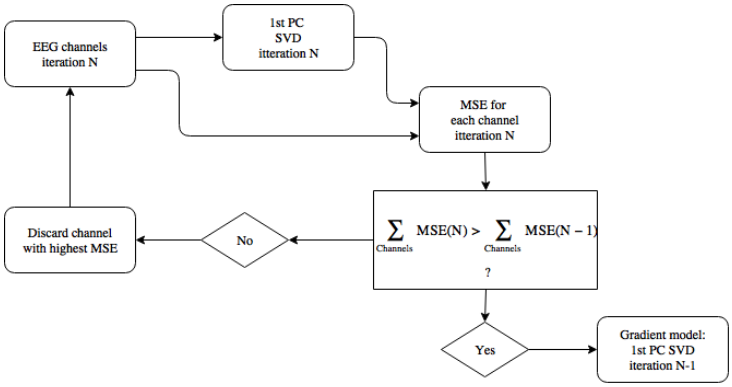

Figure 3.1: *Iteration of the algorithm that estimates the gradient waveforms* $\tilde{G}_x, \tilde{G}_y, \tilde{G}_z$.

The slice by slice regression

During a combined EEG-fMRI scan, transistor to transistor logic (TTL) trigger pulses are generated by the MR scanner to signal the acquisition of every slice. These triggers are usually used to remove the gradient artifacts that distort the EEG signal in a pre-processing phase, and must be sampled by the EEG recording system. In [4], those triggers are used to retrieve the start sample for each volume, since the estimation of the motion parameters is performed using the EEG measurement that is acquired for the whole volume.

In this project, the regression that gives the weights for each slice for every channel is performed for the corresponding fragments of the target EEG measurement and the gradient waveform models, which are given by the slice triggers. Since the sample interval between two slice triggers is much longer for the last slice in each volume than for the rest of slices in the volume, the size of the segment that is taken for the regression is the same size that is taken for the regression in the previous slice. Figure 3.2 shows how the weights w_{ix}, w_{iy}, w_{iz} for EEG channel i are calculated for a specific slice. The regression process uses the corresponding piece of the EEG gradient waveforms and the corresponding piece of the EEG target measurement according to the slice triggers to obtain the regresion weights using eq. 2.15.

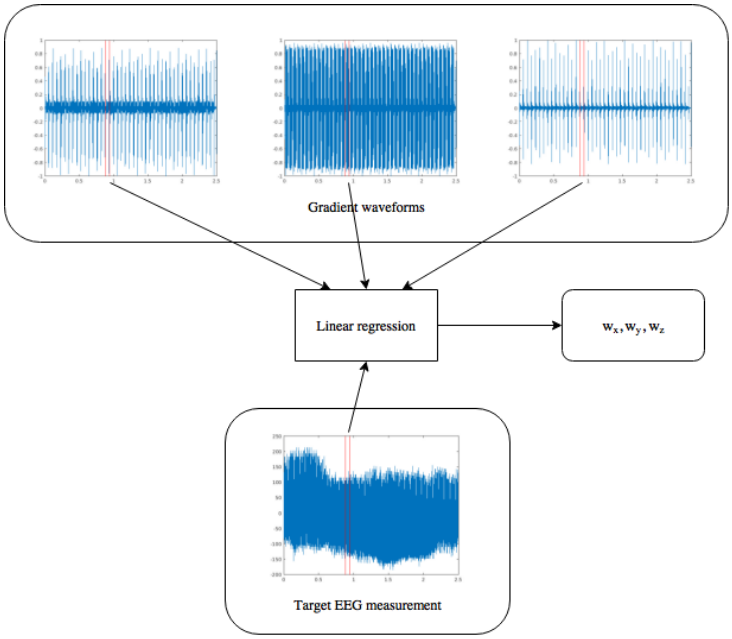

Figure 3.2: *Graphic description of how the regression weights are calculated for each slice.*

Calibration using the per-slice weights

In the regression process one set of 3xN weights (N EEG channels) is calculated for each slice in a volume, although SPM performs one motion estimation for all slices in the volume. For that reason, every set of weights that correspond to the slices that are part of a volume will be linked to the same motion parameters when the calibration matrix A is calculated through eq. 2.16.

3.2.2 Description of the data used for testing the code

Phantom measurements

Following the artificial data validation, an initial phantom setup was modified to avoid the existing wire loops that may introduce unnecessary noise, and to increase the number of channels in order to improve the performance of the calibration and testing. The initial setup consisted on a structured phantom with an EEG hood in which ten of the electrodes were pairwise interconnected to create five bipolar channels.

The described setup was modified by using silicon bolts to reinforce the connection of the paired electrodes and by increasing the number of paired electrodes up to eighteen (nine bipolar channels). The cable length was also shortened, ensured that the cable could be straight from the EEG hood to the EEG amplifier, and therefore that no extra loops where formed by a folded cable.

With the modified phantom setup, a scan was performed in a 3 tesla Philips scanner using a FLASH sequence. Thirty volumes were acquired, with 40 slices per volume. A repetition time equal to 6 ms, a flip angle of 9º and an echo time of 2.3 ms were used during the scan. The acquisition matrix dimensions were 80x80 and the field of view was 123.7x230x230 mm. The slice thickness for this data is 2.8 mm.

During the acquisition, the phantom position was modified by introducing several foam pieces between the phantom and the head coil.

Human subject measurements

For testing the performance of the motion estimation, several sets of data that were acquired before the start of this project with a human subject were used. The data were acquired on a 3 tesla Philips scanner, and they consisted of four fMRI scans using EPI sequence, while the subject was wearing an EEG hood.

Two different types of experiments were conducted to acquire this human subject data. In the first of them, the subject was asked to move only in between each volume that was was acquired. In this case, fifty volumes were acquired with a repetition time (TR) of 5 s (it took 2.5 s to acquire the volume, and there was a pause of 2.5 s to let the patient move before the acquisition of a new volume). In the second of them, the subject was asked to move continuously. In this case, one hundred volumes were acquired, and the TR was set to 2.5 s since there were no pauses during the experiment. In both experiments, forty-two slices were acquired for each volume. For these experiments the acquisition matrix dimensions were 64x64, the field of view was 192x126x192 mm, the slice thickness was 3 mm, the echo time was set to 30 ms and the flip angle was 80º.

Regarding the EEG acquisition, an EEG hood with 32 channels was used for this purpose, which was connected to a BrainVision EEG recording system, which is an MR-compatible system. The recording system was connected to an amplifier with a cutoff frequency of 1 kHz, according to the header files that were saved during the data acquisition. The EEG signals from 31 channels were saved to be used for the calibration and tests.

The sampling rate and the system bandwidth are a limitation for the acquisition of the gradient waveforms. Although they are suited for the EEG frequency band (0.5-70 Hz) [3], most of the high frequency content of the gradient waveforms are filtered away. Since the gradient switching happens very fast during the acquisition of a slice using a fast imaging technique such as EPI, the unfiltered gradient waveforms would include high frequency components that the recording system and the amplifier cannot record due to this low cutoff frequency (1 kHz).

3.2.3 Implementation issues

During the implementation of this per-slice estimation for the motion tracking, as a first approach the triggers from both the EEG measurements and the gradient waveform models were used to select the corresponding fragment of signal for the regression of each slice. However, a spike pattern appeared in the motion estimation. This pattern was repeated in certain slices over all the volumes that the motion estimation was tested for, as it can be seen in figure 3.7. In order to check if this spike pattern also appeared when other sequences were used in the acquisition, the motion estimation was performed under the same conditions (use of the triggers from both EEG measurement and gradient waveform models) for the phantom data, which were acquired using a FLASH sequence. The results do not show any spike pattern that is repeated over the volumes when the FLASH sequence is used, as it can be seen in figure 3.8. Since the motion estimation in this case contains much less noise than the motion estimation when the EPI sequence was used (figures 3.6 and 3.9), a comparison of the noise that was added in the motion estimation in both cases is performed. To evaluate the noise content in the estimation, the signal to noise ratio defined as the ratio between the actual motion that is calculated by the SPM software from the MR images and the deviation of the estimation from the actual motion is evaluated:

$$SNR = \frac{Actual\ motion}{Actual\ motion - Estimated\ motion} \tag{3.1}$$

The results for the signal to noise ratio for two different scans with a human subject with stepwise motion, which were acquired using EPI sequence, are compared in table 3.1 with the results for the scan that was performed with the phantom setup, in which a FLASH sequence is used in the acquisition, are shown.

In order to try to remove this spike pattern, only the triggers from the EEG measurements were used, and the samples that should be taken from the gradient waveform models were deduced from those triggers. The motion estimation results (fig. 3.10) show that the spike pattern was removed, but a noise pattern that was repeated over each volume was still present in the motion estimation. In order to remove this pattern, in the calibration process the values for the regression weights for each slice in the first volume were subtracted from the corresponding values of the regression weights from the rest of the volumes. When this modification was applied, this remaining pattern was reduced, as it can be seen in figure 3.11.

3.2.4 Per-slice motion for the calibration

Since SPM performs one motion realignment for the entire volume, in the calibration process for the per-slice motion estimation the weights $\Delta w_i, i = 1, .., N_{slices}$ for all the slices in a volume are associated with the same set of motion parameters Δr_h. This part of the calibration process could lead to an error in the calculation of the calibration matrix A, since the subject should be still during the acquisition of each volume during the calibration.

The use of a motion estimation method that obtains the motion parameters from the MR images for each slice would improve the accuracy of the calibration, and therefore the performance of the motion estimation.

One method of trying to emulate the per-slice motion estimation using the SPM function that performs the per-volume motion is varying the slices that are used in the realignment for each volume by using a sliding window to select the slices that are included in each of the volumes that will be realigned through SPM following the order in which the slices were acquired.

In order to implement the sliding window per-slice motion estimation through SPM, the realignment process is repeated a number of times that is equal to the number of slices that each volume contains.

For each repetition a different slice is replaced in each volume, according to the slice acquisition order. The slices from a specific volume n are replaced by the slices from the following volume $n + 1$, according to a sliding window, as it is shown in figure 3.3:

In a first step, all the slices in volume n that is used in the realignment belong to volume n in the acquisition order. In the second step, all but one will belong to volume n and one of them belong to volume $n + 1$ in the acquisition order, which is the first slice that was acquired for volume $n + 1$. In a third step, all but two will belong to volume n and two of them belong to volume $n + 1$. This process is repeated until only one slice belongs to volume n, which is the last slice that was acquired for volume n.

In each step, the SPM realignment is performed to obtain an approximation to the motion of the patient in a specific slice.

Figure 3.3 contains a three-step sequence that exemplifies how the slices are grouped into volumes to perform the per-volume realignment, when 42 slices are acquired for each volume. Each coloured group of slices represents one of the volumes, and the slices are ordered according to the first odd then even acquisition order. The grey bar under the volumes represents how the slices are grouped for the motion realignment by SPM for a specific step.

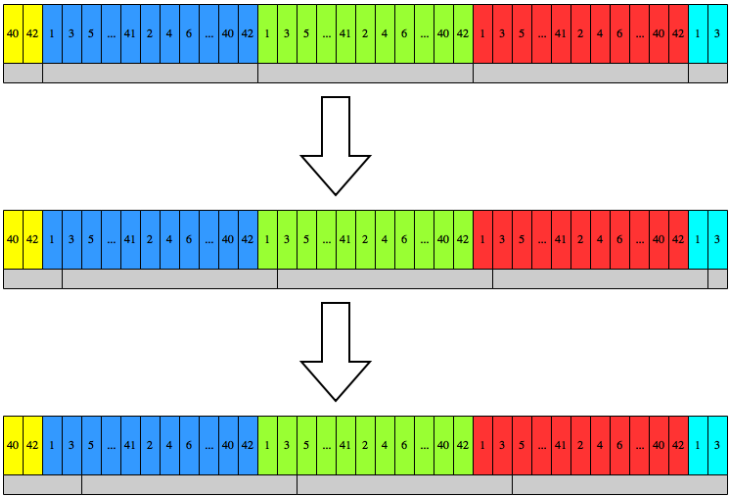

Figure 3.3: *Grouping the slices in the per-slice motion realignment.*

The sliding window per-slice estimation through SPM gives one motion estimation for each volume and for each replaced slice using the sliding window. If those motion estimations are placed sequentially according to the slice acquisition order, it is possible to obtain an approximation to a per-slice motion estimation.

Using the results from this approach to the per-slice motion estimation for the calibration, the calibration process can be modified to compare the results that are obtained using this new motion data to the motion parameters that result from the regular per-volume estimation through SPM that is performed for the calibration process that is described in subsection 3.2.1.

This per-slice estimation principle can only be tested under continuous motion, since it gives a smoothed transition between the positions in two consecutive volumes. For this reason, this per-slice calibration method will be tested with the human subject data with continuous motion that are described in section 3.2.2.

Since the slice acquisition order that was used during these scans is unknown, a method of estimating the per-slice subject position through SPM is used for three possible slice acquisition orders: ascending, first odd then even, and interleaved. An example of this motion estimation is shown in figure 3.12.

In order to decide which sequence was used, the 'smoothness' of the motion estimation was chosen as a metric, since the right slice acquisition order should give a smooth transition between the position of the subject head in consecutive volumes. This smoothness factor is determined by the second derivative of the motion parameters, since it gives how constant is the variation of them over time. For each motion parameter Δr_i, the smoothness factor will be:

$$Smoothness_i = \sum \frac{\partial^2 \Delta r_i}{\partial t^2} \tag{3.2}$$

A constant variation of the motion parameter Δr_i would result in a low smoothness. Thus, the decision criterion to find the most probable acquisition order will be that the slice acquisition order with the lowest smoothness factor will be chosen as the slice acquisition order. Table 3.2 shows the results for the smoothness for the tree tested slice acquisition orders during two different scans with continuous subject motion. The slice order that was selected to be the most probable acquisition order is the ascending order, since it gives the lowest results for the smoothing factor.

Using the per-slice motion realignment that is implemented through SPM, the acquired data were tested and the results that are obtained through this modified calibration are compared in figure 3.12 with the motion estimation that results from the calibration using a constant motion parameter for all the slices in the volume as it is described in subsection 3.2.1.

3.3 Results

Figure 3.4 shows a comparison for the results of the gradient model estimation for the gradient along the x direction $\tilde{G}_x$ by using the first component of the SVD and by using an average over the channels. For this estimation, the signal from 31 EEG channels is used, and the channels that have been used are also displayed in the figures. The first component of th SVD and the channel waveforms are normalized to their variance for a better understanding of the results. The results for the estimation of the gradient waveforms in y and z directions are shown in appendix A.

Figure 3.5 contains the accumulated mean square error for all the channels that are used for the modeling of the gradient waveforms $\tilde{G}_x, \tilde{G}_y, \tilde{G}_z$ through the first component of the singular value decomposition (SVD) , using the iterative algorithm that is described in 3.2.1. The accumulated mean square error is represented for the different number of channels that are used for the gradient waveform estimation. The EEG data that are used in figures 3.4 and 3.5 were acquired during a MR pre-scan for three runs, in which only one gradient in one of the directions in space is active during each run, respectively.

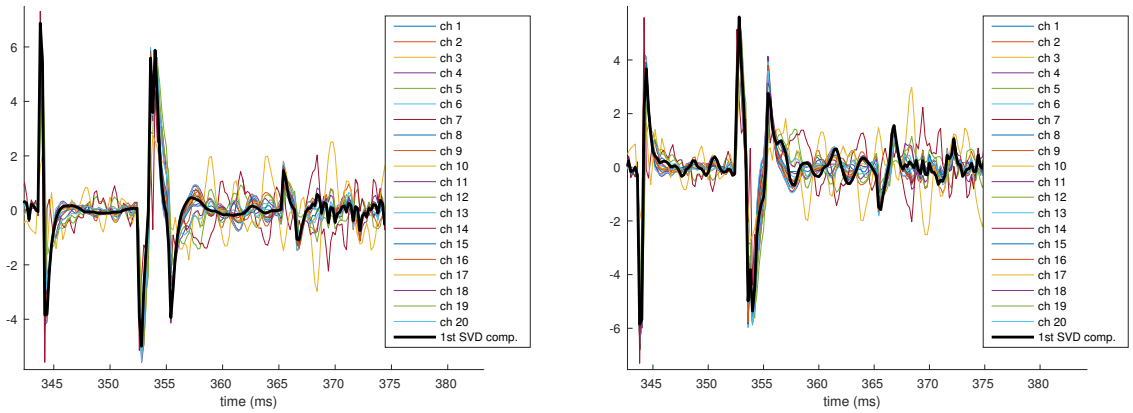

(a) *Gradient modeling through SVD.* (b) *Gradient modeling through channel averaging.*

Figure 3.4: *$\tilde{G}_x$ estimation and channels that are used for this purpose.*

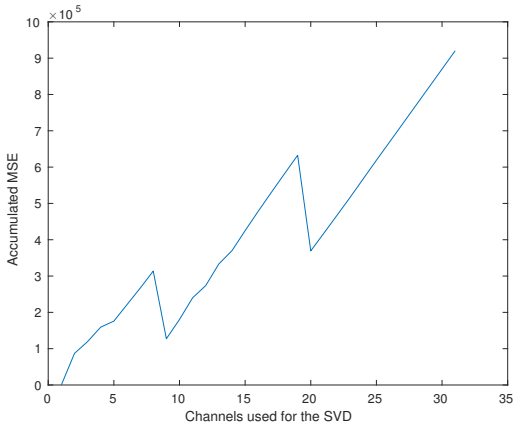

(a) *Estimation of G_x.*

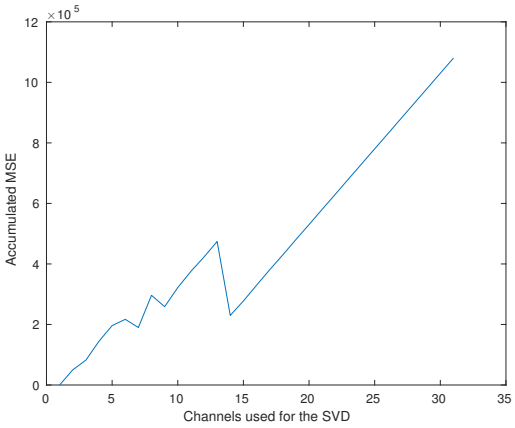

(b) *Estimation of G_y.*

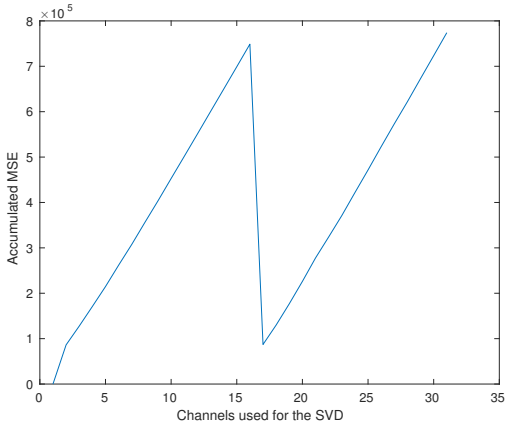

(c) *Estimation of G_z.*

Figure 3.5: *Accumulated MSE for different number of channels that are used in the gradient waveform estimation.*

Figure 3.6 shows a comparison between the per-slice and per-volume estimation for the six motion parameters (three translation parameters t_x, t_y, t_z and three rotation parameters r_x, r_y, r_z) for three of the volumes that are used for the testing of the per-slice motion estimation. Only the triggers from the EEG target measurement are used, and the subtraction of the per-slice regression weights of the first volume has been performed. The results from the per-volume motion estimation are repeated for each slice in the volume to compare them to the per-slice estimation results.

In figure 3.7 the slice-volume presentation of the per-slice motion estimation for the parameter that represents the rotation around the x direction r_x for the 24 volumes that are used to test the per-slice estimation. Both triggers from the gradient waveforms and the EEG target measurement are used, and the subtraction of the per-slice regression weights of the first volume has not been performed. The spike pattern that is repeated over the volumes can be observed in this figure. For figures 3.6 and 3.7, the dataset that has been used was acquired during the experiments with a human subject with stepwise motion using EPI sequence, which is described in subsection 3.2.2. Neither post-processing nor filtering has been applied to the motion estimation in both figures.

The results from the previous figures can be compared with the results from figures 3.8 and 3.9, which show the results for the slice-volume motion estimation for the parameter that defines the rotation around the x axis (r_x) when two triggers are used, and the comparison between the per-slice and per-volume estimation for three of the volumes that have been tested. The data that are used in this case was acquired during the sessions using the phantom setup that is described in subsection 3.2.2, using a FLASH sequence. For the results that are displayed in those figures the per-slice estimation has not been post-processed or filtered. When a FLASH sequence is used in the acquisition, no spike pattern is repeated in the per-slice motion estimation, and this estimation is much less noisy than the motion estimation that is obtained when EPI sequence is used. The signal to noise ratio (SNR) for the motion estimation for two different scans using EPI sequence is compared with the SNR results when a FLASH sequence is used. The SNR that is obtained for the motion estimation when a FLASH sequence is used is significantly higher than the SNR that results from the use of an EPI sequence in the acquisition.

If figures 3.10 and 3.11 are compared, the reader can evaluate the improvement in the motion estimation results when the regression weights for the first volume in the calibration are subtracted from the regression weights from the rest of the volumes. The noise pattern that is repeated in the motion estimation over each volume in figure 3.10 is reduced through this subtraction, as it can be seen in figure 3.11. The data that have been used for these figures is the same data that are used for figures 3.6 and 3.7.

The units for the translation motion parameters are in millimetres (mm) and the units for the rotation motion parameters are in radians for all the figures that are presented.

The slice-volume representations of the results that are shown in this section for the r_x parameter are shown for the rest of the motion parameters in appendix A.

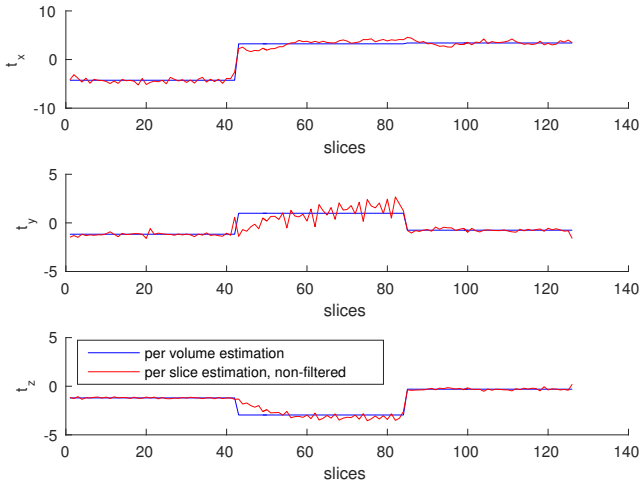

(a) *Motion estimation for the translation parameters.*

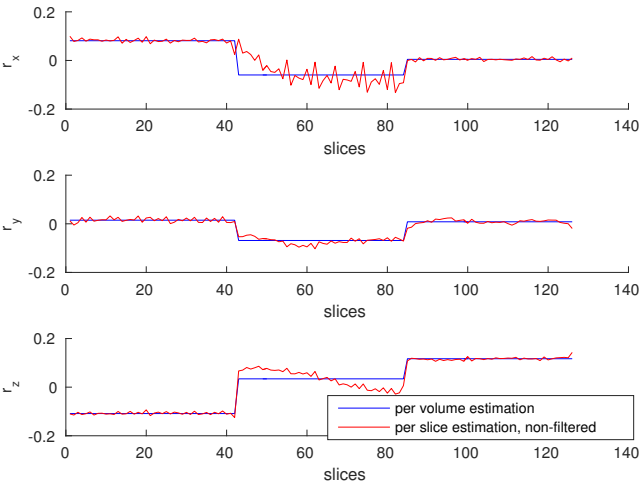

(b) *Motion estimation for the rotation parameters.*

Figure 3.6: *Comparison between per-volume and per-slice estimation (EPI sequence).*

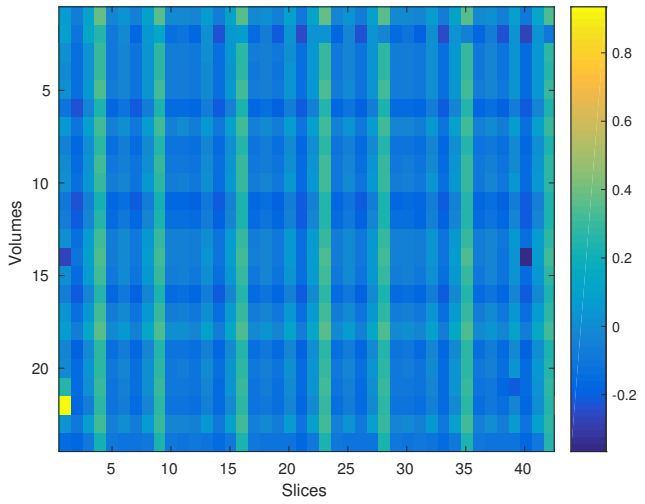

Figure 3.7: *Slice-volume representation for the motion estimation of r_x (EPI sequence) using both triggers.*

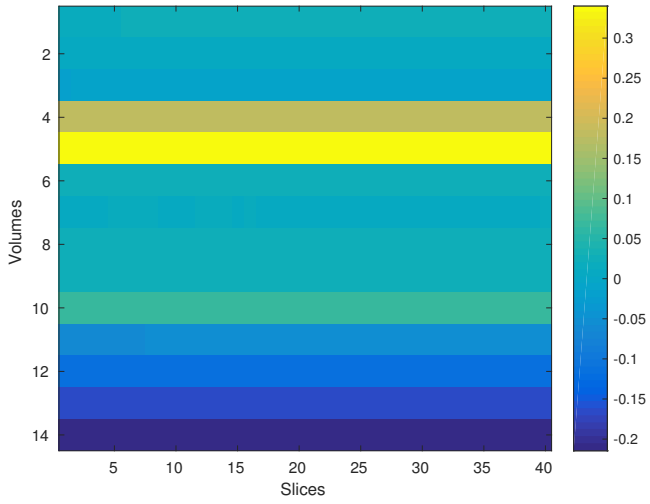

Figure 3.8: *Slice-volume representation for the motion estimation of r_x (FLASH sequence) using both triggers.*

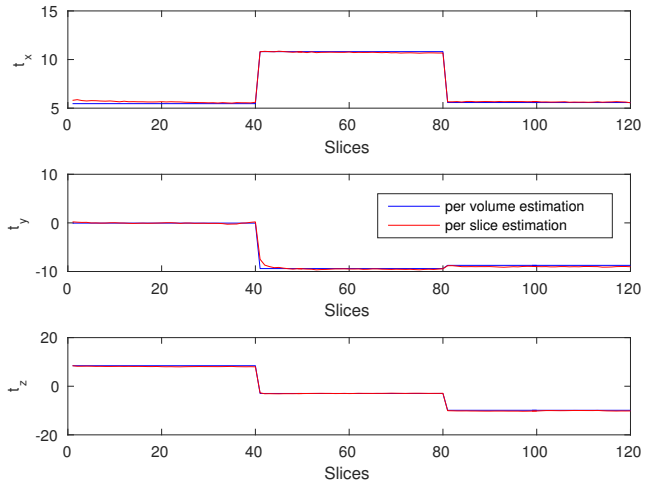

(a) *Motion estimation for the translation parameters.*

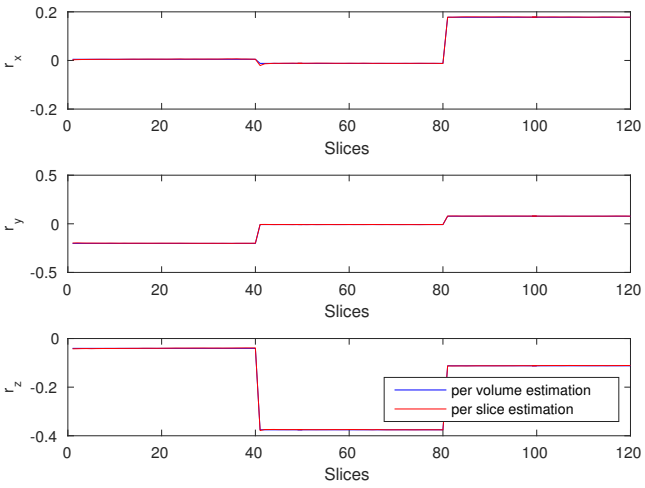

(b) *Motion estimation for the rotation parameters.*

Figure 3.9: *Comparison between per-volume and per-slice estimation (FLASH sequence).*

Table 3.1: *SNR for the motion estimation using EPI and FLASH sequences.*

	EPI scan 1	**EPI scan 2**	**FLASH scan**
SNR	2.02×10^5	4.34×10^5	1.71×10^6

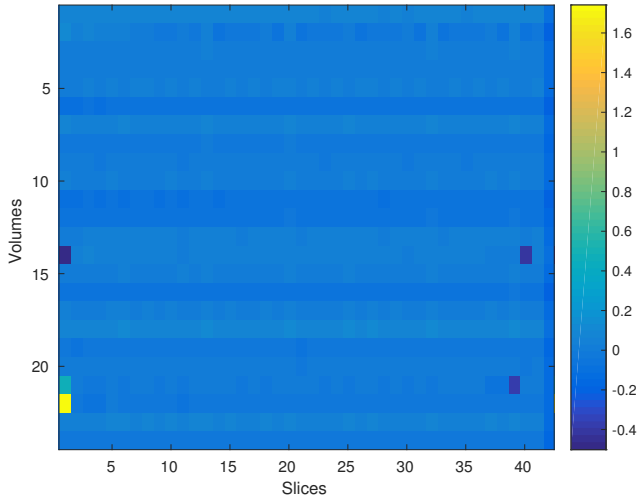

Figure 3.10: *Slice-volume representation for the motion estimation of r_x (EPI sequence) using the triggers from the EEG measurement.*

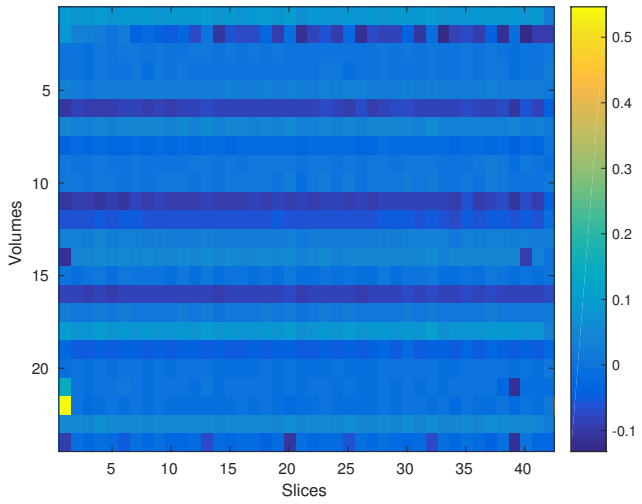

Figure 3.11: *Slice-volume representation for the motion estimation of r_x (EPI sequence) using the triggers from the EEG measurement, after the volume subtraction.*

In figure 3.12 a comparison of the results for the per-slice realignment method using the SPM software as it is described in subsection 3.2.4 is shown for the mentioned slice acquisition orders (ascending, first odd then even, and interleaved). Those results are compared with the regular per-volume estimation using SPM that is used in the calibration process that is described in subsection 3.2.1.

Since the slice order that is actually used in the acquisition of the MR images should be the acquisition order with the lowest smoothness factor (as it is defined in eq. 3.2), the results for the average smoothness over all the slices are shown for the six motion parameters from two different MR scans in table 3.2. In figure 3.13 the motion estimation results for the six motion parameters with this new calibration method are compared with the results that are obtained when the regular calibration is used. The MR images for the realignment and the EEG data are taken from one of the datasets with a human subject with continuous motion, which are described in 3.2.2. No post-processing or filtering has been performed to the motion estimation results.

The units for the translation motion parameters are in millimetres (mm) and the units for the rotation motion parameters are in radians for figures 3.12 and 3.13.

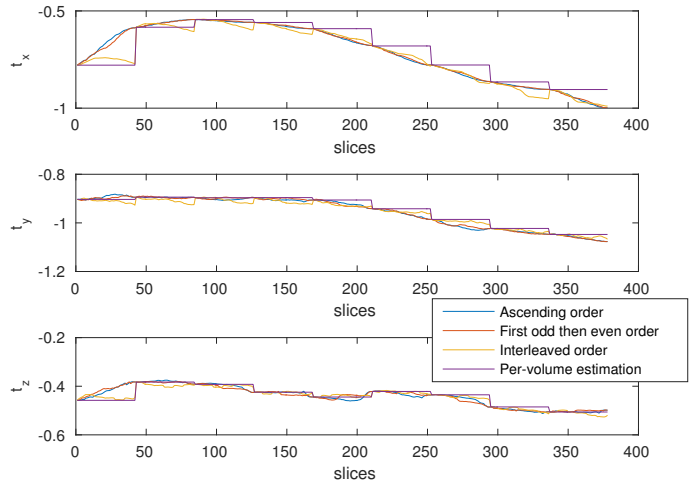

(a) *Motion estimation for the translation parameters.*

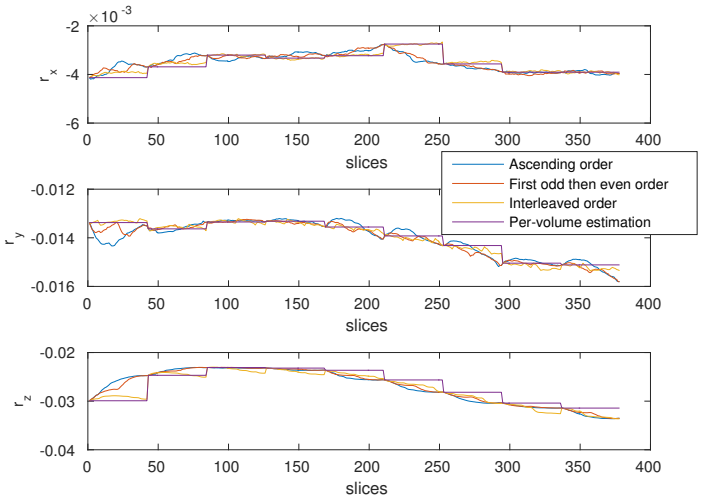

(b) *Motion estimation for the rotation parameters.*

Figure 3.12: *Motion estimation for several slice acquisition orders.*

Table 3.2: *Results for the smoothness factor for different slice acquisition orders.*

(a) *Smoothness factor, first scan.*

Parameter	Ascending	First odd then even	Interleaved
$\mathbf{t_x}$	4.46	4.17	31.67
$\mathbf{t_y}$	4.57	4.94	10.54
$\mathbf{t_z}$	4.51	4.71	9.45
$\mathbf{r_x}$	0.15	0.17	0.62
$\mathbf{r_y}$	0.11	0.12	0.28
$\mathbf{r_z}$	0.15	0.18	0.92

(b) *Smoothness factor, second scan.*

Parameter	Ascending	First odd then even	Ascending
$\mathbf{t_x}$	4.21	3.56	17.71
$\mathbf{t_y}$	5.43	6.16	13.67
$\mathbf{t_z}$	5.3	5.43	10.88
$\mathbf{r_x}$	0.22	0.25	0.92
$\mathbf{r_y}$	0.11	0.11	0.26
$\mathbf{r_z}$	0.13	0.12	0.48

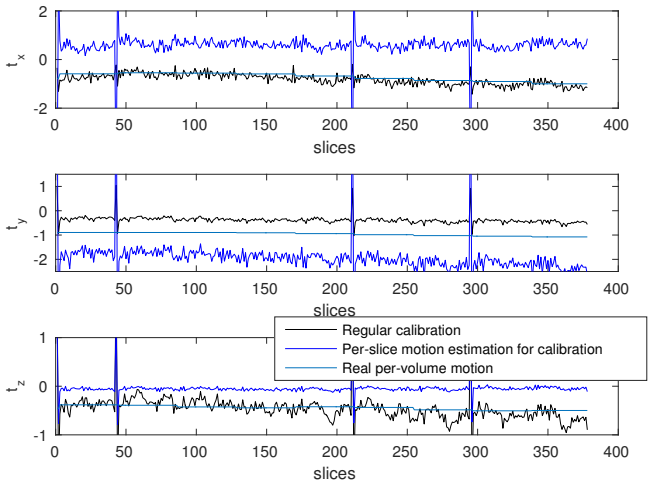

(a) *Motion estimation for the translation parameters.*

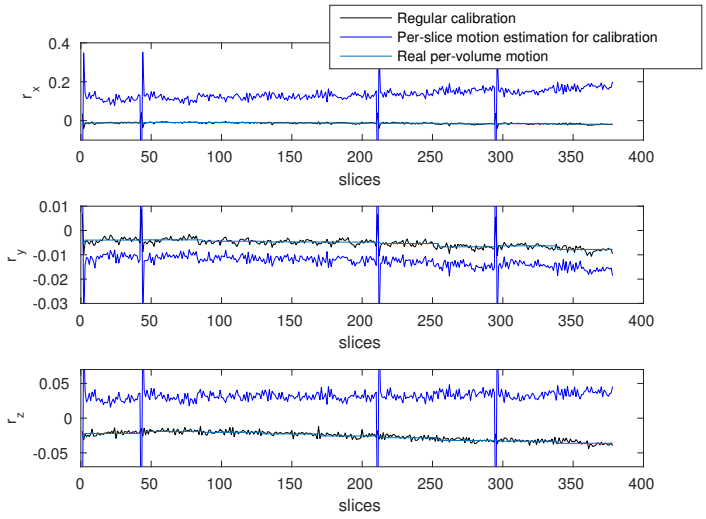

(b) *Motion estimation for the rotation parameters.*

Figure 3.13: *Motion estimation when using the per-volume estimation in the calibration and when using the per-slice estimation approach.*

3.4 Discussion and conclusion

As it was expected, a measurement noise is generated during the motion estimation process due to the small amount of samples that is used in the regression for each slice, due to the limited sampling rate of the EEG recording system (5 kHz) and the partitioning process that is performed to the gradient waveform and the target EEG measurement to estimate the motion in each slice.

Use of slice triggers for the regression

Unlike it was expected in a first approach to the per-slice estimation, optimal results were obtained when only the slice triggers from the measured EEG signals were used for the regression instead of using both the slice triggers from the gradient waveforms and the slice triggers from the EEG measurement to find out the fragment of each signal that should be used for the regression of each slice. When the slice triggers from both signals were used, a spike pattern appeared in the results for the motion estimation for every volume. If only the slice triggers from the measured EEG signal are used, this slice pattern is removed.

This different outcome in the motion estimation is due to the fact that, besides that the inter-slice trigger interval is not constant because the time between slices is not an integer number of EEG samples, the slice triggers for two different scans are not synchronized.

The trigger pulses that are used to signal each slice during the scan follow the transistor-to-transistor logic (TTL) that is defined by a high level voltage when slice is signaled by the scanner. Those TTL pulses are generated with a short high-level duration that cannot be detected through the relatively low sampling frequency of the EEG measurement system. To be able to detect those trigger pulses, they must be are prolonged by an external circuit, which may decrease the signal to noise ratio of the pulses that are generated by the MR scanner. A hypothesis for this non-synchronized slice trigger pulses from different scans is that this noisy pulses that result from the TTL pulse prolongation may lead to a variation in the sample in which the pulse detection is made.

However, since the inter-volume sample interval, which is equal to the repetition time (TR) in single-shot EPI, is an integer number of samples, the EEG system is synchronized with the scanner clock, so the triggers for the first slice of each volume will be synchronized.

After applying the per-slice estimation to the data that were acquired from the measurements with the phantom setup, which were acquired with a FLASH sequence with a longer volume acquisition time (18.5 s for the FLASH sequence instead of 2.5 s for the EPI sequence), it was found that the spike pattern that appeared for the per-slice estimation using EPI sequence did not appear using FLASH sequence although the slice triggers from both the EEG measurement and the gradient waveform models were used. This might be due to the fact that the time between slices is an integer number of EEG samples, so the triggers in both scans would be synchronized.

To analyze the performance of per-slice estimation with data that are acquired using a different sequence, the translation and rotation parameters that result from the motion estimation are displayed for three of the volumes that are used for testing the per-slice estimation (fig. 3.9). The per-slice motion estimation results that are obtained using a FLASH sequence are much less noisy than the per-slice estimation when data from a scan that uses an EPI sequence. This could be caused by the higher amount of data that are used in the regression for each slice (2315 samples for FLASH sequence against 294 samples for EPI sequence). Another factor that could contribute to this much less noisy estimation are the improved phantom setup, which avoids unnecessary wire loops between the EEG hood and the EEG amplifier, or the fact that the stepwise motion experiments were performed with a human subject, who may have moved unconsciously during the acquisition of each volume.

Regarding the motion estimation with the data that were acquired using a human subject, after the spike pattern was compensated by using only the triggers from the EEG measurements, another noise pattern appeared. This pattern was also repeated over each volume, and it specially affected the results for the last slice of each volume (figure 3.10).

This pattern is removed by subtracting the regression weights for each slice in the first volume acquired in the calibration from the corresponding slices in the following volumes. This first volume is considered to have no motion, since it is used a reference as well in the statistical parametric model (SPM) during the motion estimation(figure 3.11).

However, the motion estimation for the first volume contains some random noise, that will be introduced as a noise pattern to the per-slice estimation in the rest of the volumes. This pattern is partially removed by the filtering process that is described in chapter 4.

The calibration

As it has been stated in section 3.2.4, the calibration process could be a source or error. In the first part of the calibration when the EEG measurements while a gradient along one direction is active in each run for the gradient waveform estimation, the subject must not move for the gradient model to be reliable.

In addition, also as part of the calibration in the regression process one set of 3xN weights is calculated for each slice in a volume, and SPM performs one motion estimation for the entire volume. Because of this fact, the weights for all the slices that correspond to the same volume will be linked in the calibration to the same motion when the A matrix is calculated. Therefore, if the subject moves during the acquisition of a volume, the calibration process will introduce additional error.

When the calibration is modified by introducing the results of the per-slice realignment that is performed through SPM, the motion estimation results are not improved, but become worse, as it can be seen in figures 3.13. This may be caused by the fact that the motion estimation is distorted for the slices in the middle of the volume, since for these slices the realignment uses fairly the same number of slices from two consecutive volumes. This fact may deteriorate the calibration process, and therefore the motion estimation. Thus, the calibration process should be improved through another method of estimating the subject motion for each slice using the MR images, as it is stated in the areas of future work that are suggested in chapter 5.

Chapter 4

Real time filtering of the motion estimation

In this chapter different alternatives to the filtering of the tracking parameters that result from the per-slice motion estimation are analyzed in order to reduce the noise that is generated during the estimation. The real-time application of the motion tracking makes the Kalman filter algorithm a suited method for the smoothing of the motion estimation. The implementation and testing of the Kalman filter are described in this chapter.

4.1 Introduction

Due to the limited sampling rate in the EEG system (5 kHz) and the partitioning process that is performed to the gradient waveform and the target EEG measurement to estimate the motion in each slice, the result of the per-slice motion estimation presented in chapter 3 contains some noise. Therefore, this noisy approach to the subject motion must be smoothed before the motion is compensated in the scanner in order to minimize the changes in the scanner parameters while a volume is being scanned.

The unknown nature of this noise involves the use of an adaptive filter that should be able to minimize the noise in the estimation. Besides, the real-time purpose of the per-slice motion estimation demands the use of an algorithm that should be able to perform an estimation of the current position and orientation of the subject based on previous observations.

The Kalman filter has been broadly used in navigation and motion tracking [24, 21], where the state of a dynamic system must be estimated from noisy or incomplete observations. In these situations, the Kalman filter uses probabilistic inference to estimate the past, present and future state of a random process by minimizing the mean square error in the estimation. In order to perform the estimation, a model of the system should be provided to the algorithm [6, 19, 22].

4.2 Methodology

4.2.1 The Kalman filter

The Kalman filter is a recursive algorithm that corresponds to the solution to the Bayesian filtering equations described in [11] for the linear estimation or filtering of the state of a discrete random process with the following prediction and correction steps. It is based on a discrete time-variant state-space model that is represented by these two equations:

$$x_k = F_k x_{k-1} + w_k \tag{4.1}$$

$$y_k = H_k x_k + v_k \tag{4.2}$$

where:
x_k is the state that is being estimated at time k. In the context of the application of the Kalman filter in this project, the filtering is applied to the per-slice motion estimation parameters, although it can be also applied to the weights that result from the per-slice regression from the gradient waveforms and the EEG measurement.
y_k is the measurement at time k.
$w_k \sim N(0, Q_k)$ is the process noise: the error made in the estimation of the current state based on the previous state by assuming a specific state transition for the dynamic model. It is the error made when the motion in time k is estimated from the motion in time $k-1$.
$v_k \sim N(0, R_k)$ is the measurement noise: the error made in the estimation of the actual measurement given the state transition model and the measurement model. It is the difference between the real motion and the estimated motion.
w and v are assumed to be statistically independent.
F_k is the transition matrix of the dynamic model, which is assumed to be constant (no motion), except for a random component, for this smoothing application.
H_k is the measurement model matrix. In this project, the actual motion should be equal to the estimated motion under no measurement error.

All w_k, v_k, F_k, H_k are assumed to be stationary over time. However, the process noise and the measurement noise can be updated on the fly based on new input motion parameters that result from the per-slice estimation.

Given the initial estimate as the expected value of x_0, since it minimizes the error made in the first estimation:

$$\hat{x}_0 = E[x_0] \tag{4.3}$$

The covariance matrix for the initial estimation is:

$$P_0 = E[(x_0 - \hat{x}_0)(x_0 - \hat{x}_0)^T] \tag{4.4}$$

For each input sample at time step $k = 1, 2, 3, ...$, at the prediction step the current state and the error covariance are defined as:

$$\hat{x}_{k|k-1} = F_k \hat{x}_{k-1} \tag{4.5}$$

$$P_{k|k-1} = F_k P_{k-1} F_k^T + Q \tag{4.6}$$

After predicting the current state based on the previous state, the Kalman gain matrix K_k is estimated and the current state $\hat{x}_k$ is updated:

$$K_k = P_{k|k-1} H_k^T (H_k P_{k|k-1} H_k^T + R)^{-1} \tag{4.7}$$

$$\hat{x}_k = \hat{x}_{k|k-1} + K_k(y_k + H_k \hat{x}_{k|k-1}) \tag{4.8}$$

$$P_k = P_{k|k-1} - K_k H_k P_{k|k-1} \tag{4.9}$$

The Q and R matrices are the covariance matrices of the measurement noise and the process noise, respectively:

$$Q \sim E[w_k w_k^T] \tag{4.10}$$

$$R \sim E[v_k v_k^T] \tag{4.11}$$

4.2.2 Dynamic model specification and parameters

For the application of the Kalman filter in this project, which is the smoothing of the result of the per-slice motion estimation, the F matrix is defined as the identity matrix, since the current state is assumed to be equal as the previous state during the acquisition of a certain volume, except for some process noise w_k, which is the random motion of the subject between two consecutive slices. This movement is assumed to be relatively small between consecutive time steps.

The H matrix is also established as an identity matrix since the current state is the estimation of the current measurement in each time k. Thus, the measurement should be equal to the current state, except for some measurement noise v_k that should be removed.

Regarding the covariance matrices for the measurement noise R and the process noise Q, as a first approach the R matrix is defined as a diagonal matrix containing the variance of the error between the known data from the calibration, given by the SPM motion estimation, and the input data of the filter, given by the per-slice estimation, for each tracking parameter. The estimation of this error is performed from the data that are acquired in the first ten volumes in the calibration phase. As a first approach the Q matrix is defined as a diagonal matrix containing the variance of the estimation of the motion parameters for the data that are acquired during the calibration phase.

In a second step, the described diagonal matrices were replaced by the actual covariance matrices calculated from the sama data that were used to estimate the variance of the process noise and the measurement noise in the first approach.

Given those specifications, the prediction step equations can be reduced to:

$$\hat{x}_{k|k-1} = \hat{x}_{k-1} \tag{4.12}$$

$$P_{k|k-1} = P_{k-1} + Q \tag{4.13}$$

The update step equations can also be reduced:

$$K_k = P_{k|k-1}(P_{k|k-1} + R)^{-1} \tag{4.14}$$

$$\hat{x}_k = \hat{x}_{k|k-1} + K_k(y_k + \hat{x}_{k|k-1}) \tag{4.15}$$

$$P_k = P_{k|k-1} - K_k P_{k|k-1} \tag{4.16}$$

4.2.3 Filter tuning. The smoothing factor

According to [23] the smoothing effect of the filter can be modified by scaling the covariance matrices of the process noise Q and the measurement noise R.

$$R = k_v \bar{R} \tag{4.17}$$

$$Q = k_w \bar{Q} \tag{4.18}$$

where $\bar{R}$ and $\bar{Q}$ are the matrices of unit norm that contain the structure of the respective noise processes.

In [23] a smoothing factor S is defined as the quotient of both multiplying factors:

$$S = \frac{k_w}{k_v} \tag{4.19}$$

Through this scaling factor, it is possible to control the effective smoothing of the filter. An increment in the quotient will increase the smoothing effect, while a decrement in it will decrease the smoothing.

4.2.4 The Kalman smoother

Among other alternatives to the Kalman filter that are presented in the literature, there is a Kalman smoother algorithm [17], which provides better results than the Kalman filter algorithm at smoothing the input data.

The Kalman smoother algorithm uses a forward-backward algorithm to smooth the input data by updating all past states and state probabilities using each new imput measurement. The smoothing algorithm is implemented in two steps: the forward pass and the backward pass.

- At time T, when measurements $x_1, x_2, ..., x_{T-1}$ are available, the forward pass consists on estimating the new state in time T, $\hat{x}_T$ and the covariance matrix P_T of the estimated state given the past measurements. This step is implemented as a regular Kalman filter estimation, since it gives both state estimation and covariance matrix for each time.

- The backward pass consists on updating each estimated state x_t and covariance matrix P_t given all estimations from the future $x_{t+1}, x_{t+2}, ..., x_T$, starting from the most recent estimation.

  First, the likelihood of the estimation is calculated from the state transition matrix and the covariance matrix at each time:

  $$L_t = P_{t|t} F^T P^{-1}_{t+1|t} \tag{4.20}$$

  The backward state update is performed using the likelihood of the estimation in the current time:

  $$\hat{x}_{t|T} = \hat{x}_{t|t} + L_t(\hat{x}_{t+1|T} - \hat{x}_{t+1|t}) \tag{4.21}$$

  $$P_{t|T} = P_{t|t} + L_t(P_{t+1|T} - P_{t+1|t})L_t^T \tag{4.22}$$

Although the backward pass in the Kalman smoother provides an extra estimation that is supposed to improve the performance at smoothing the input motion parameters than the regular Kalman filter, the Kalman smoother is a non-causal algorithm that uses measurements from the future to perform a forward-backward filtering of the input data.

The role of the filter or the smoother that is applied to the result of the per-slice motion estimation in this project is the filtering of the noise from the estimation in real-time, since the scanner should be updated in real-time during the scan to perform the prospective motion correction. Thus, the smoothing needs to be performed by a causal filter, and therefore the Kalman smoother algorithm is not used in this project.

4.2.5 Simulated data

Since the acquisition of new sets of data is time consuming and the motion parameters cannot be controlled as an input (it is difficult to control how the subject moves between the acquisition of each slice), simulated motion data were created for validation purposes to emulate the result of the noisy per-slice motion estimation. To create the artificial data, the stepwise motion human subject dataset that is described in subsection 3.2.2 was used.

To build the simulated data, first, the calibration is performed using the measured gradient waveforms and the measured EEG waveforms that were acquired during the experiments with a human subject through the same procedure that is described in subsection 2.5 for the acquired data from the sessions with a human subject. The artificial EEG waveforms are created from the calibration matrix and the desired artificial motion parameters through eq. 2.16. After this, noise is added to these EEG signals to simulate the noise that is introduced during the scan and in the slice estimation process, which should be removed by the filtering. The noisy motion parameters are estimated to generate the simulated data that will be used to test the filtering algorithm.

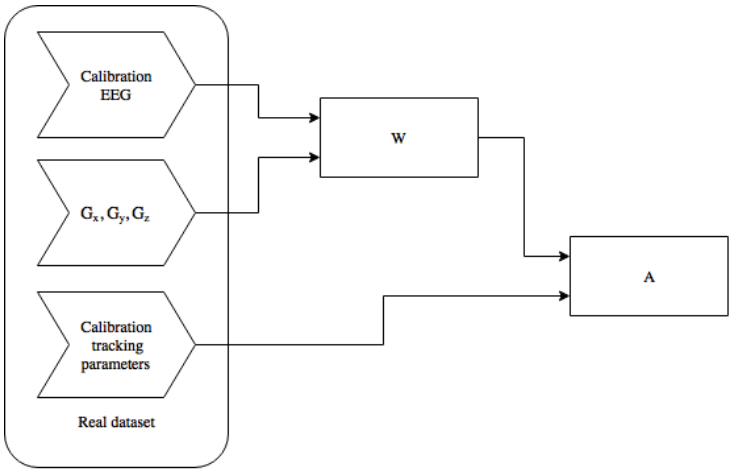

Figure 4.1: *Calibration process as it is described in section 2.5.*

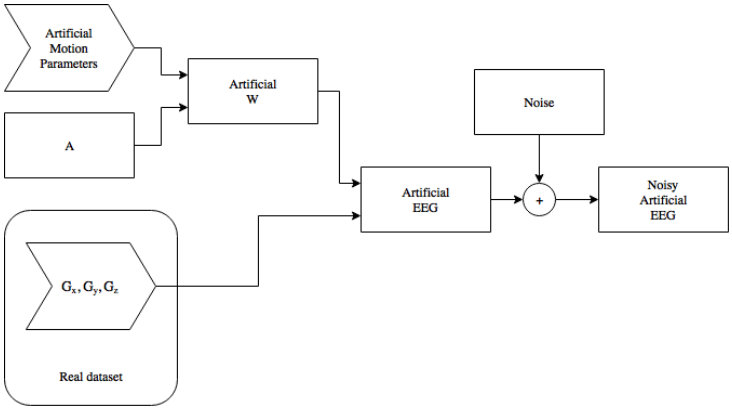

Figure 4.2: *Obtaining of the noisy artificial EEG waveforms. Noise is introduced to the artificial EEG waveforms according to the desired signal to noise ratio.*

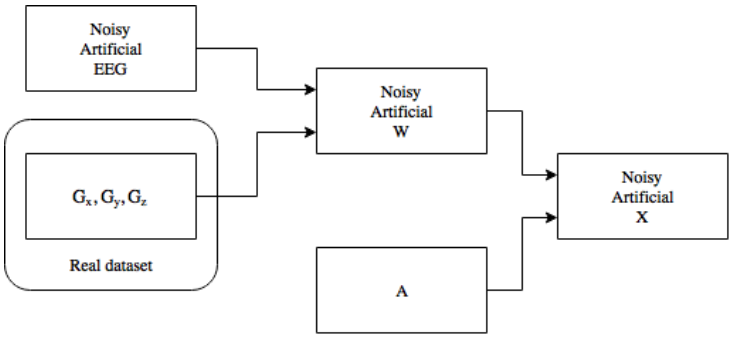

Figure 4.3: *Estimation of the motion parameters from the noisy artificial EEG waveforms.*

4.2.6 Non-modeled motion. Outlier detection

Despite its good performance under the assumed state transition model, the Kalman filter is very sensitive to modeling errors since it takes into account all previous observations and estimations in the estimation of the current state due to its infinite impulse response nature. When sudden motion happens, it is expected that the high frequency content that the sudden motion implies will produce an error on the smoothing, since this sharp change in the motion parameters will turn into a smooth transition until the filter recovers from the error.

Outlier values may also affect the performance of the filter in a similar way as sudden motion does. Outliers might appear as a result of the misalignment between the slice triggers from the EEG measurements and the gradient waveforms that are used during the regression, or from fragments of EEG signal that have a low signal to noise ratio.

To improve the smoothed estimation of the motion that the filter provides, the outliers must be detected and removed. Since the Kalman filter is broadly used for tracking purposes, and outliers often appear in systems that use Kalman filter algorithms, several solutions for outlier detection and removal are presented in the literature.

A modified version of the Kalman filter that introduces a weighted version of the input observations is described in [20]. This weights and the system dynamics are updated in each time step using by using a maximum likelihood criterium. This method avoids the need of a parameter tuning from the user. In [5] modification of the Kalman filter algorithm that is robust against outliers and system uncertainties is presented. In this method, the state transition matrix is modified to include unknown but bounded parameter uncertainties in the dynamic model. In [12] a Kalman-like algorithm that assumes that the measurement error may come from either one or two normal distributions, and the state transition is determined by a Markov Chain. The current state in estimated as a weighted average of the estimates from two parallel filters where the weights are calculated from the posterior probabilities. The state transition model that is proposed in [2] involves a dynamic model with data that are corrupted not only with Gaussian noise, but with other probability distributions such as heavy tailed distributions, which increases the flexibility of the model under the presence of outliers in the input data.

In this project, the outlier detection is performed using the variance of the estimated measurement noise for each motion parameter, which is included in the diagonal of the covariance matrix of the measurement noise that is estimated for the Kalman filter. When the per-slice motion estimation is much higher than the subject can naturally move between the acquisition of two consecutive slices (about 58 ms for the EPI sequence that has been used in the data acquisition), the input estimation is considered as an outlier.

To detect outliers in the motion estimation, each input parameter is compared to the median value of the previous three input parameters. If the motion difference between the two estimations is higher than four times the standard deviation of each parameter, the sample is detected as an outlier and it is replaced by the median value of the previous three input parameters.

This outlier detection method would introduce a delay of at most one sample in the smoothed estimation in case of sudden motion of the patient.

4.2.7 Evaluation of the effect of the Kalman filter

For a quantitative assessment of the performance of the Kalman filter, different metrics have been used. The motion estimation results that are used for this purpose are the motion parameters that result from the estimation using the human subject data with stepwise motion that are described in 3.2.2. The first of them is the variance of the motion results, which is calculated for each volume. Table 4.1 shows the results for the average of this variance over the volumes that are used for testing the code for each of the motion parameters.

Since the results of the filtering may distort this variance for the results in the first slices of each volume if sudden motion happens, smaller fragments of the motion results were taken to calculate this variance. Tables 4.2, 4.3 and 4.4 show the results for the average of the variance that is calculated for segments of 6, 10 and 21 slices, respectively.

Another factor that can be evaluated to assess the performance of the filtering is the accumulated error that is generated by the filtering in the first half of each volume as a result of the smoothing effect when sudden motion happens. For this purpose, the filtering results are compared to the per-volume estimation results to obtain an accumulated error for the first half of each volume, since the difference between the real motion and the filtered motion should be higher in this interval. Table 4.5 shows an average of this accumulated error over the volumes for each motion parameter.

4.3 Results

In figure 4.4 the results of the Kalman filtering that is applied to the per-slice motion estimation parameters are shown for different values of the smoothing factor S. The filter was applied to the artificial data that are created for the validation of the filter, which are described in subsection 4.2.5. The units for the translation and rotation motion parameters are in mm and radians, respectively.

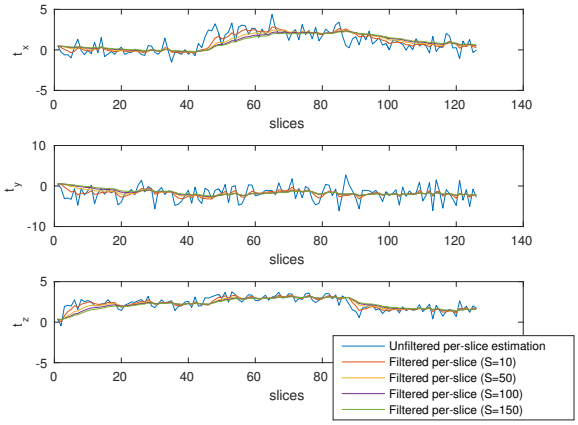

(a) *Filtered motion estimation for the translation parameters.*

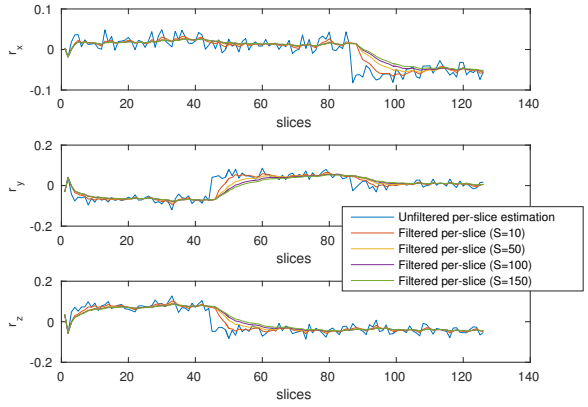

(b) *Filtered motion estimation for the rotation parameters.*

Figure 4.4: *Comparison of the filtering performance with different values of smoothing factor.*

Figure 4.5 shows the improvement of the outlier detection in the filtered data for three of the volumes that have been used to test the code. When outlier values are present in the motion estimation, the smoothing effect of the Kalman filter is disturbed by those outliers. The implemented outlier detection is able to remove those outlier motion estimations before the data are filtered. The data that were used for testing the performance of the Kalman filter under the pressence of outlier estimations is the human subject data with stepwise motion that are described in 3.2.2. The units for the translation parameters are in mm and the units for the rotation parameters are in radians.

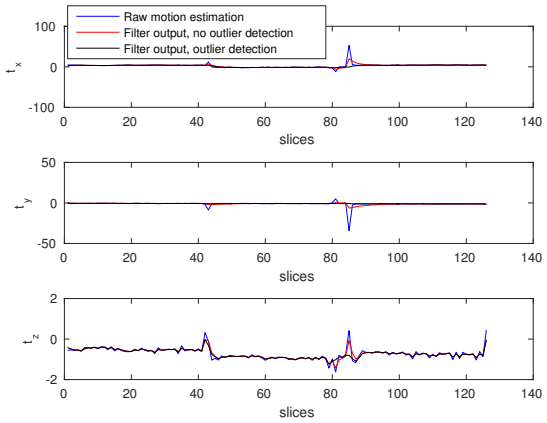

(a) *Filtered motion estimation for the translation parameters* t_x, t_y, t_z.

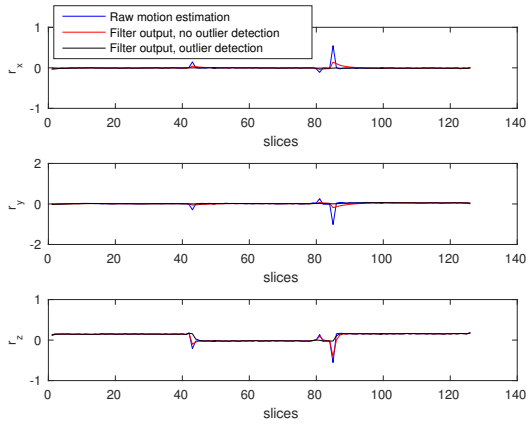

(b) *Filtered motion estimation for the rotation parameters* r_x, r_y, r_z.

Figure 4.5: *Performance of the Kalman filter under outliers.*

Tables 4.1, 4.2, 4.3, 4.4 and 4.5 show the results for the average variance and the maximum error for the assessment of the performance of the filtering that is described in subsection 4.2.7. The results are presented first for the raw motion estimation and the motion estimation when the outlier removal algorithm is applied. The results are also displayed for the filtered motion estimation with different values of the smoothing factor.

Table 4.1: Variance of the estimation results over each volume.

	Unfiltered		Filtered				
	Raw estimation	**Outlier detection**	**S = 10**	**S = 50**	**S = 100**	**S = 150**	**S = 500**
$\mathbf{t_x(mm^2)}$	3.19	0.29	0.26	0.27	0.31	0.34	0.52
$\mathbf{t_y(mm^2)}$	1.415	0.090	0.047	0.044	0.048	0.051	0.057
$\mathbf{t_z(mm^2)}$	0.029	0.027	0.025	0.022	0.021	0.021	0.024
$\mathbf{r_x(rad^2)}$	5.72×10^{-4}	1.90×10^{-4}	1.24×10^{-4}	1.26×10^{-4}	1.51×10^{-4}	1.72×10^{-4}	2.58×10^{-4}
$\mathbf{r_y(rad^2)}$	1.53×10^{-3}	9.66×10^{-5}	6.83×10^{-5}	6.55×10^{-5}	6.99×10^{-5}	7.41×10^{-5}	8.96×10^{-5}
$\mathbf{r_z(rad^2)}$	7.25×10^{-4}	1.96×10^{-4}	1.93×10^{-4}	1.91×10^{-4}	1.95×10^{-4}	2.03×10^{-4}	2.58×10^{-4}

Table 4.2: *Variance of the estimation results over a fragment of six slices.*

	Unfiltered		**Filtered**				
	Raw estimation	**Outlier detection**	$S = 10$	$S = 50$	$S = 100$	$S = 150$	$S = 500$
$t_x(mm^2)$	3.12	0.23	0.18	0.16	0.15	0.14	0.11
$t_y(mm^2)$	1.36	0.065	0.018	0.0094	0.0071	0.0059	0.0034
$t_z(mm^2)$	0.021	0.018	0.015	0.011	0.0095	0.0086	0.0070
$r_x(rad^2)$	5.17×10^{-4}	1.40×10^{-4}	6.29×10^{-5}	4.27×10^{-5}	4.02×10^{-5}	3.84×10^{-5}	2.95×10^{-5}
$r_y(rad^2)$	1.53×10^{-3}	8.00×10^{-5}	4.05×10^{-5}	2.22×10^{-5}	1.65×10^{-5}	1.37×10^{-5}	7.79×10^{-6}
$r_z(rad^2)$	6.76×10^{-4}	1.48×10^{-4}	1.44×10^{-4}	1.39×10^{-4}	1.39×10^{-4}	1.42×10^{-4}	1.56×10^{-4}

Table 4.3: *Variance of the estimation results over a fragment of ten slices.*

	Unfiltered		**Filtered**				
	Raw estimation	**Outlier detection**	**S = 10**	**S = 50**	**S = 100**	**S = 150**	**S = 500**
$\mathbf{t_x(mm^2)}$	3.87	0.70	0.61	0.48	0.42	0.38	0.27
$\mathbf{t_y(mm^2)}$	1.41	0.089	0.040	0.023	0.017	0.014	0.0079
$\mathbf{t_z(mm^2)}$	0.052	0.049	0.046	0.039	0.036	0.033	0.025
$\mathbf{r_x(rad^2)}$	6.79×10^{-4}	3.06×10^{-4}	2.18×10^{-4}	1.61×10^{-4}	1.37×10^{-4}	1.23×10^{-4}	8.24×10^{-5}
$\mathbf{r_y(rad^2)}$	1.55×10^{-3}	1.23×10^{-4}	7.76×10^{-5}	4.89×10^{-5}	3.77×10^{-5}	3.19×10^{-5}	1.86×10^{-5}
$\mathbf{r_z(rad^2)}$	1.23×10^{-3}	7.53×10^{-4}	7.35×10^{-4}	6.84×10^{-4}	6.41×10^{-4}	6.08×10^{-4}	4.87×10^{-4}

Table 4.4: *Variance of the estimation results over a fragment of 21 slices.*

	Unfiltered		**Filtered**				
	Raw estimation	**Outlier detection**	**S = 10**	**S = 50**	**S = 100**	**S = 150**	**S = 500**
$\mathbf{t_x(mm^2)}$	3.19	0.28	0.24	0.24	0.27	0.29	0.40
$\mathbf{t_y(mm^2)}$	1.40	0.073	0.029	0.023	0.023	0.024	0.022
$\mathbf{t_z(mm^2)}$	0.026	0.024	0.022	0.018	0.017	0.016	0.018
$\mathbf{r_x(rad^2)}$	5.47×10^{-4}	1.66×10^{-4}	9.65×10^{-5}	9.31×10^{-5}	1.09×10^{-4}	1.22×10^{-4}	1.59×10^{-4}
$\mathbf{r_y(rad^2)}$	1.55×10^{-3}	9.60×10^{-5}	6.80×10^{-5}	6.27×10^{-5}	6.26×10^{-5}	6.23×10^{-5}	5.51×10^{-5}
$\mathbf{r_z(rad^2)}$	6.80×10^{-4}	1.54×10^{-4}	1.51×10^{-4}	1.50×10^{-4}	1.55×10^{-4}	1.63×10^{-4}	2.19×10^{-4}

Table 4.5: *Accumulated error made in the estimation in the first half of each volume.*

	Unfiltered		**Filtered**				
	Raw estimation	**Outlier detection**	**S = 10**	**S = 50**	**S = 100**	**S = 150**	**S = 500**
$\mathbf{t_x(mm)}$	4.06	1.66	8.75	8.88	9.29	9.73	12.62
$\mathbf{t_y(mm)}$	2.83	0.92	3.86	4.12	4.51	4.86	6.64
$\mathbf{t_z(mm)}$	0.56	0.54	1.83	1.76	1.77	1.80	2.01
$\mathbf{r_x(rad)}$	0.064	0.033	0.13	0.14	0.17	0.19	0.31
$\mathbf{r_y(rad)}$	0.090	0.026	0.159	0.157	0.160	0.165	0.205
$\mathbf{r_z(rad)}$	0.063	0.041	0.147	0.144	0.145	0.149	0.176

4.4 Discussion and conclusion

Non-modeled motion

The smoothing effect that the Kalman filter introduces to the motion estimation can be controled by a tunable parameter, the smoothing factor. However, as it is stated in section 4.2.6, the Kalman filter is very sensitive to non-modeled motion such as sudden motion or outlier values that result from the estimation.

Sudden motion in the estimation is turned into smoothed transitions, which follow an exponential curve from the previous estimated position until it converges in the current estimated position. The convergence rate depends on the value of the smoothing factor, as it can be seen in figure 4.4.

Since the purpose of the Kalman filter is the smoothing of the noise that is present in the motion estimation, the effect of the smoothing factor in the Kalman filter represents a tradeoff between the smoothing of the motion estimation and the error that is introduced when sudden motion happens. Since in a realistic situation the subject is not expected to move much between two consecutive slices, the probability of sudden motion to happen is very low, so the smoothing can be increased without making big errors in the filtered estimation.

Outlier values disturb the smoothing by creating an exponential response in the output of the filter, which also depends on the smoothing factor. The effect of the filter under the pressence of outlier values in the motion estimation is visible in figure 4.5. As it can be seen, the effect of these outliers is successfully removed by the algorithm that is described in subsection 4.2.6.

Performance of the filter

The noisy data are tested with several values of the scaling factor to compare the performance of the filtering. As it is stated in [23], the higher this smoothing factor is the more smoothing effect is achieved. However, since the Kalman filter should quickly adapt to motion in real-time, there is a tradeoff between the smoothing results and the adaptative performance of the filter.

Since the results for the average of the variance are distorted if the variance is applied to a high number of slices (tables 4.1 and 4.4), the smoothing effect of the Kalman filter can be clearly observed when the outlier-free unfiltered motion estimation is compared with different filtered versions of the motion estimation. As it can be seen in tables 4.2 and 4.3, when the smoothing factor increases, the variance of the estimation decreases, and therefore the smoothing effect of the filter is higher.

On the other hand, as it can be seen in table 4.5 the error in the estimation that is caused by the filtering due to the sudden motion is higher when the smoothing factor increases. Therefore, there is a tradeoff between the smoothing effect that is achieved and the error that is introduced due to sudden motion of the patient. This tradeoff can be contoled by the smoothing factor, according to the type of motion data: in a regular application of this per-slice motion tracking system, the patient would move continuously, and therefore the error that is introduced by sudden motion would be less important than the smoothing effect. For that situation, a high smoothing factor would be selected to maximize the smoothing effect.

Chapter 5

Future work

Due to the limited time extension of this thesis and some external issues that have happened during the development of the project, such as the unability to synchronize the MR scanner with the NeuroOne EEG system, which was established as one of the objectives of this thesis at the beginning of it, some of the topics that could be adressed if there was more time to continue with this project are presented in this chapter.

5.1 Use of an improved EEG acquisition system

The NeuroOne EEG recording system allows the acquisition of measurements during an MR scan, as the BrainVision recording system that has been used in this thesis does. This recording system can be used to try to improve the motion estimation, since it is able to work with up to 64 EEG channels instead of the 32 that the BrainVision recording system that has been used during the experiments with human subjects can work with.

Besides the number of channels that can be used, the NeuroOne recording system is able to work with a higher sampling rate, which increases the number of samples that are used in the regression for each slice (in the scans that have been performed using the BrainVision EEG recording system, the sampling rate that has been used is 5 kHz, and the NeuroOne EEG recording system can acquire up to 16000 samples per second). According to the per-slice motion estimation results that are obtained using the data from the experiments with the phantom setup, which uses a FLASH sequence that involves the acquisition of 2315 EEG samples per slice instead of the 294 samples per slice that are acquired using EPI, this could give a less noisy estimation, and should help to avoid the non-synchronization of the triggers since the TTL pulses would be sampled with a higher sampling rate as well, and maybe even avoiding the use of the circuit for the prolongation of the TTL pluses to detect them.

In addition to this, since the filters of the BrainVision recording system limit the bandwidth of the gradient waveforms, the use of a new EEG acquisition system with higher bandwidth would help to improve the estimation of the gradient waveforms and therefore the accuracy of the calibration.

5.2 Improving the accuracy in the calibration

Since the per-slice approach to the image realignment for the calibration that is proposed and implemented in this thesis introduces a higher amount of error than the regular per-volume image realignment, another robust method of estimating the patient motion for each slice using the MR images could be investigated as a subject of future work in order to improve the accuracy in the calibration process.

5.3 The prospective motion correction system

After the implementation of this slice by slice motion tracking method, it should be included in a prospective motion correction system that would update the scanner parameters before the acquisition of each slice. Two processes sould be performed in real-time to implement the prospective motion correction.

In the first place, the EEG measurements should be acquired by the routine that performs the motion tracking in real time. The BrainVision recorder allows to pass the EEG data to other programs on the local computer or to other computers via TCP/IP through the remote data access (RDA) function that is included in the recording system. After it is configured, the data are sent from the EEG recorder, which acts as a server, to the real-time routine that performs the tracking, which acts as a client. The RDA functions are available on Python, C++ and Matlab [1].

Secondly, the scanner parameters should be updated in real-time according to the tracking information. For this purpose, Philips developed an eXTernal Control (XTC) application that allows the user to control the scanner esternally by introducing real-time adjustments, such as updating the FOV [18].

Since Matlab is not very extended for real-time acquisition and processing purposes, Python was selected at the beginning of this project to perform the real-time regression and motion estimation. Unfortunately, since this thesis has a limited time extension and the other project aims were considered as more important for the overall development of this thesis, only an analysis of how the EEG data would be acquired and processed in real-time through the RDA Python libraries was performed.

Due to the fact that the calibration can be performed offline, the inversion of A matrix that is used to estimate the motion Δr_h according to eq. 2.16 can be calculated before the scan. Since the gradient waveform models are estimated during the calibration process, the inversion of the matrix that contains the variation of the gradient waveforms $\frac{\partial \tilde{G}_x(t)}{\partial t}, \frac{\partial \tilde{G}_y(t)}{\partial t}, \frac{\partial \tilde{G}_z(t)}{\partial t}$ that is used in eq. 2.15 can be performed before the beginning of the scan as well. The implementation of the Kalman filter estimation also requires a matrix inversion for the calculation of the Kalman gain, but since the filter is applied to six motion parameters (three translation parameters t_x, t_y, t_z and three rotation parameters r_x, r_y, r_z), the inversion requires a relatively low computational load.

Chapter 6

Conclusions

In this thesis a real-time motion tracking algorithm for a prospective motion correction system during magnetic resonance imaging has been described and tested.

As a first step, several motion tracking techniques that are used for tracking the motion of the patient during magnetic resonance imaging have been analyzed, focusing in those techniques that can be used in a prospective motion correction system.

Secondly, an existing motion estimation method that uses the artifacts that are measured by an EEG equipment during the MR scan is used to estimate the motion of the patient for every slice. Several issues that have appeared during the implementation of the motion estimation have been addressed and satisfactory results have been obtained from this motion estimation method.

In parallel with the analysis and implementation of the per-slice motion estimation, a Kalman filter algorithm has been implemented to remove unwanted noise components that may have been introduced in the motion estimation, and at the same time to estimate in real-time the motion of the patient according to past observations. The smoothing effect that is achieved through the Kalman filter can be modified according to the motion of the patient. Since the Kalman filter is sensitive to non-modeled motion, a modification of the Kalman filter that is able to detect and remove outlier values in the motion estimation is proposed and tested in this thesis.

Unfortunately, not all the aims that were established at the beginning of this project have been fulfilled, such as the real-time implementation of the tracking algorithm in Python, or the updating of the calibration matrix on-the-fly using the motion data that is acquired during the scan. However, some of the goals that were proposed have been fulfilled, and also other topics that were not considered at the beginning of the project have been addressed to a large extent during this project.

Appendix A

Additional results

A.1 Estimating the gradient waveforms

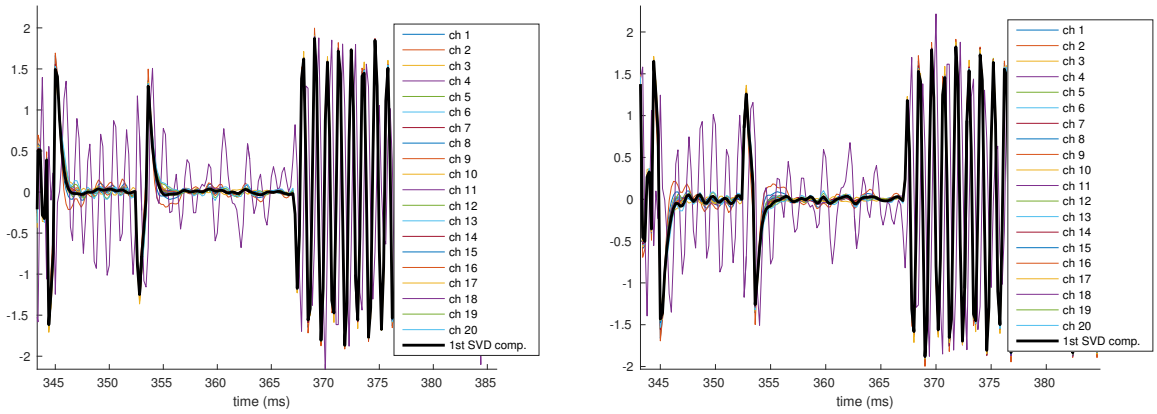

(a) *Gradient modeling through SVD.* (b) *Gradient modeling through channel averaging.*

Figure A.1: *$\tilde{G}_y$ estimation and channels that are used for this purpose.*

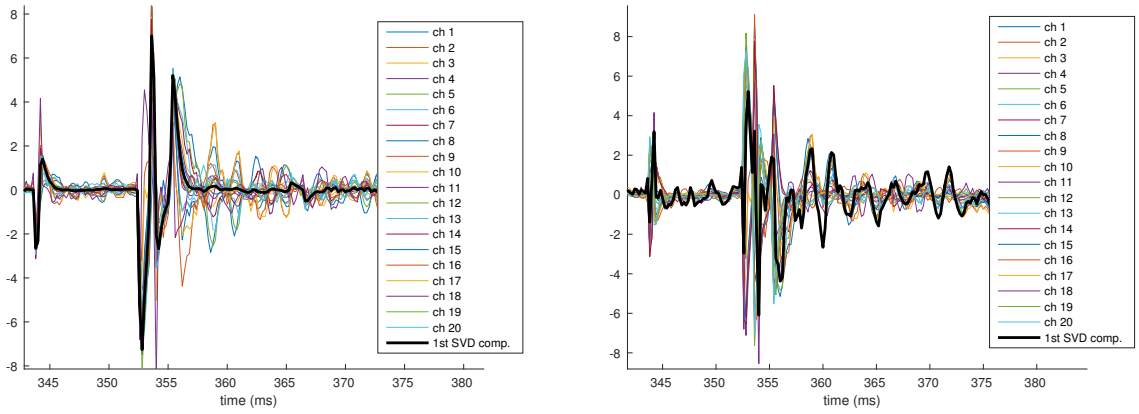

(a) *Gradient modeling through SVD.* (b) *Gradient modeling through channel averaging.*

Figure A.2: *$\tilde{G}_z$ estimation and channels that are used for this purpose.*

A.2 Per-slice motion estimation

A.2.1 Results when two triggers are used, EPI sequence

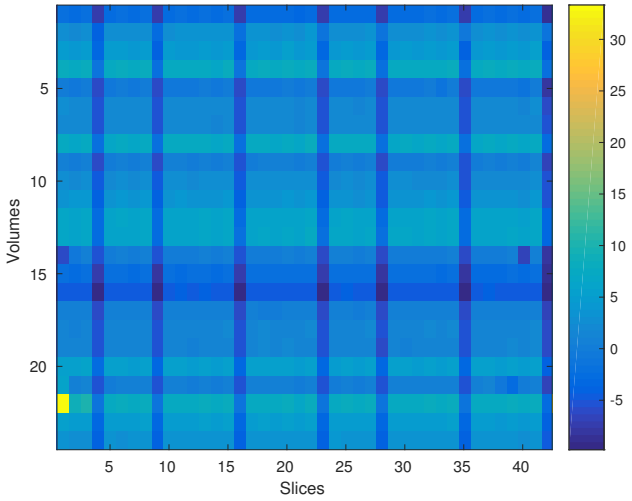

Figure A.3: *Slice-volume representation for the motion estimation of t_x (EPI sequence) using both triggers.*

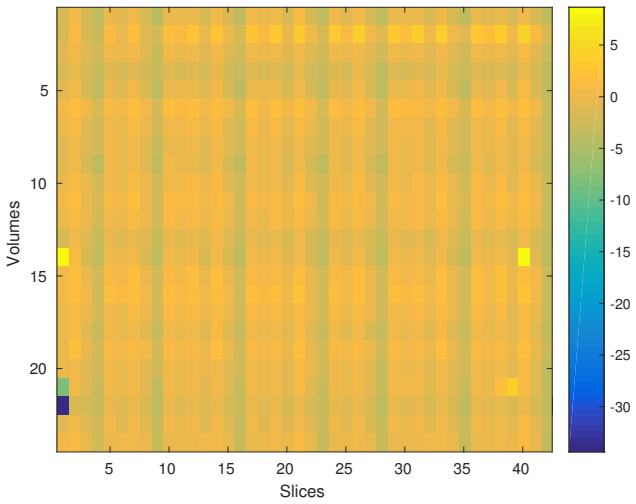

Figure A.4: *Slice-volume representation for the motion estimation of t_y (EPI sequence) using both triggers.*

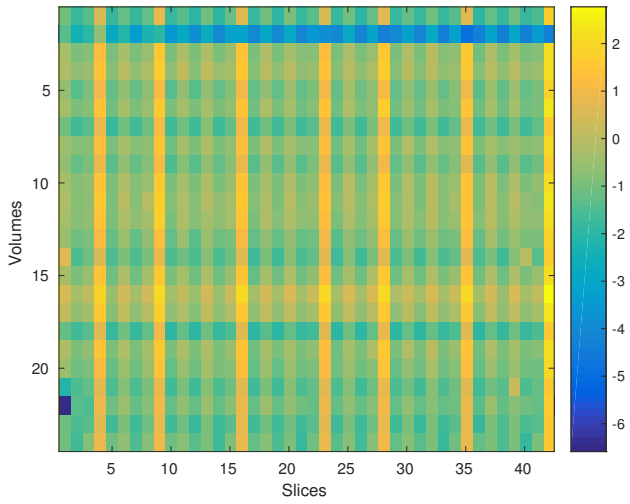

Figure A.5: *Slice-volume representation for the motion estimation of t_z (EPI sequence) using both triggers.*

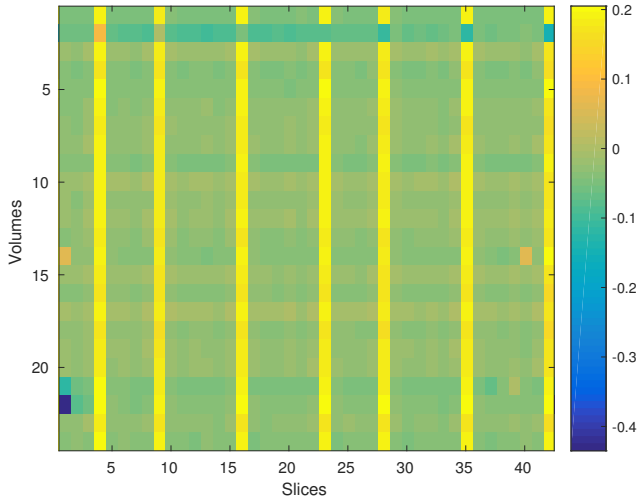

Figure A.6: *Slice-volume representation for the motion estimation of r_y (EPI sequence) using both triggers.*

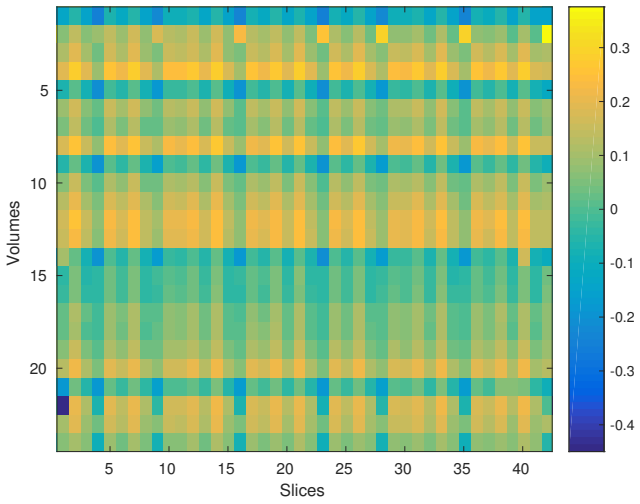

Figure A.7: *Slice-volume representation for the motion estimation of r_z (EPI sequence) using both triggers.*

A.2.2 Results when two triggers are used, FLASH sequence

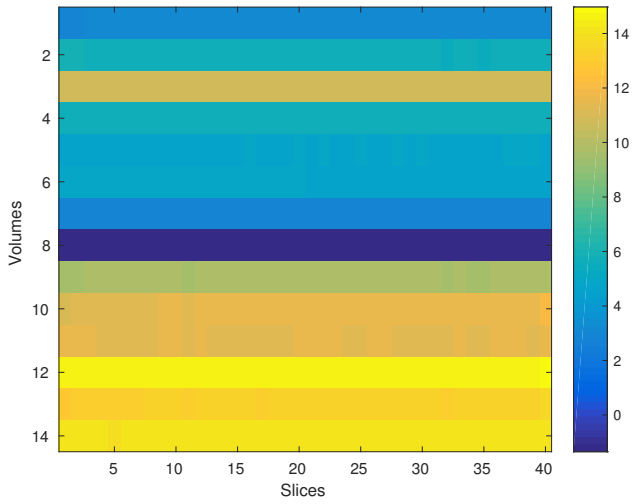

Figure A.8: *Slice-volume representation for the motion estimation of t_x (FLASH sequence) using both triggers.*

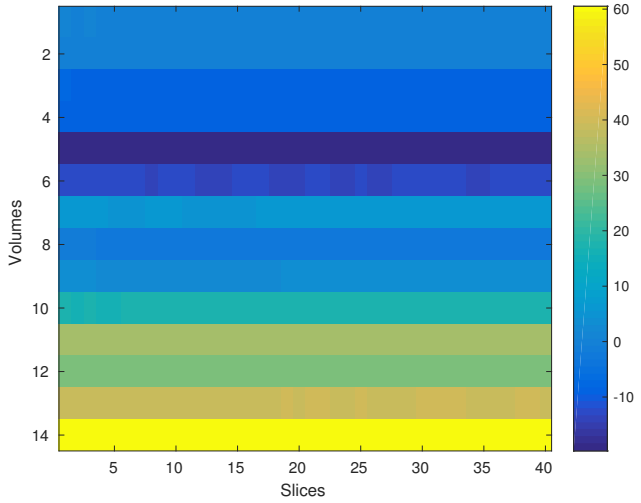

Figure A.9: *Slice-volume representation for the motion estimation of t_y (FLASH sequence) using both triggers.*

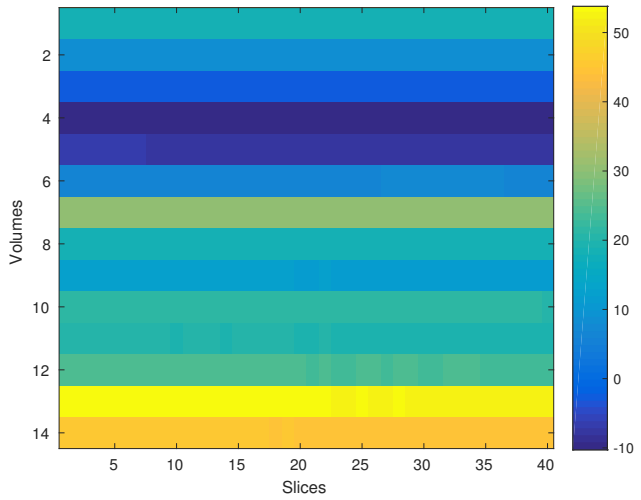

Figure A.10: *Slice-volume representation for the motion estimation of t_z (FLASH sequence) using both triggers.*

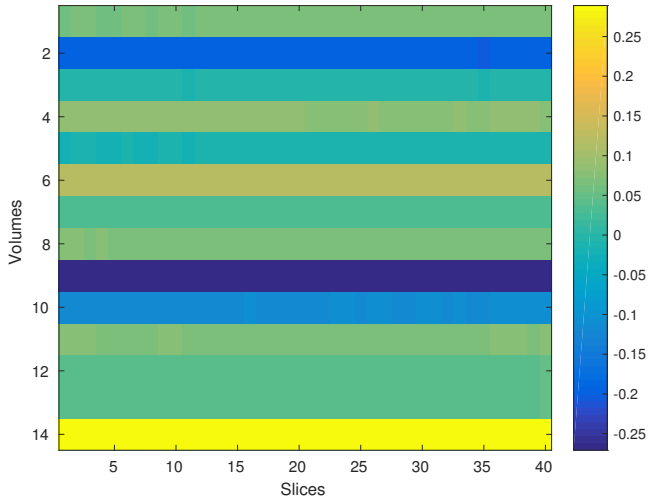

Figure A.11: *Slice-volume representation for the motion estimation of r_y (FLASH sequence) using both triggers.*

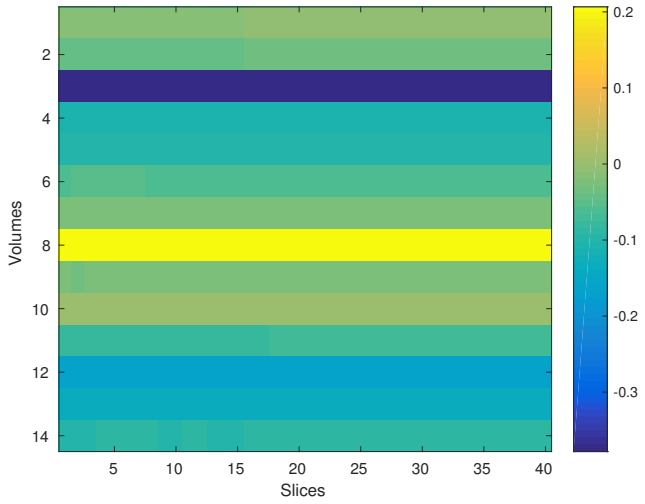

Figure A.12: *Slice-volume representation for the motion estimation of r_z (FLASH sequence) using both triggers.*

A.2.3 Results when one trigger is used, without subtraction of the regression weights

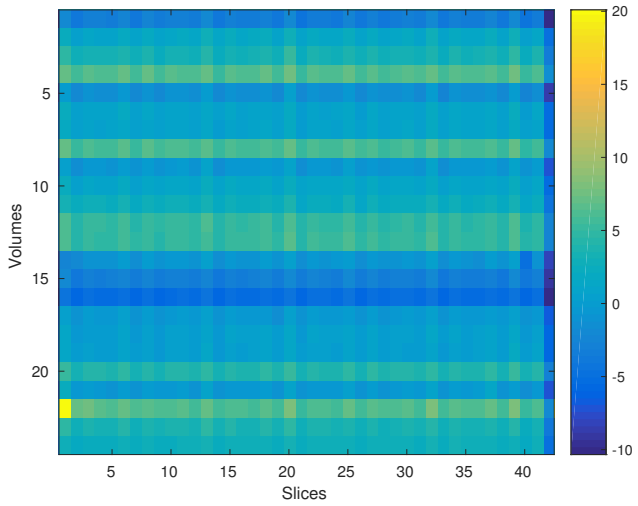

Figure A.13: *Slice-volume representation for the motion estimation of t_x (EPI sequence) using the triggers from the EEG measurement.*

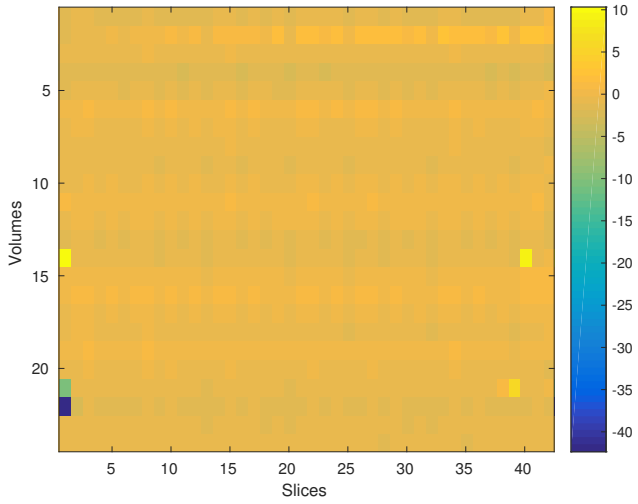

Figure A.14: *Slice-volume representation for the motion estimation of t_y (EPI sequence) using the triggers from the EEG measurement.*

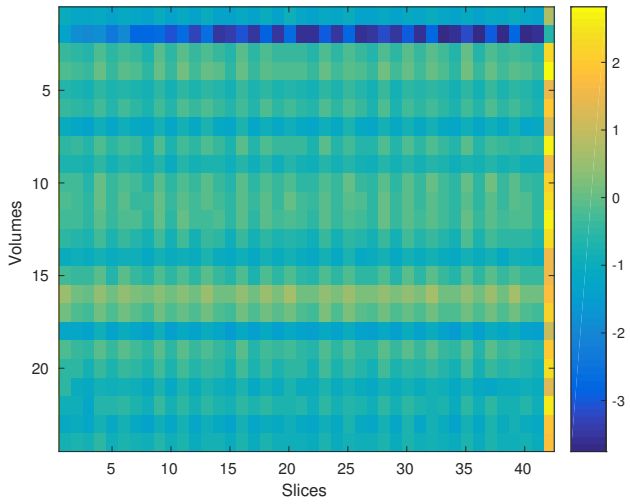

Figure A.15: *Slice-volume representation for the motion estimation of t_z (EPI sequence) using the triggers from the EEG measurement.*

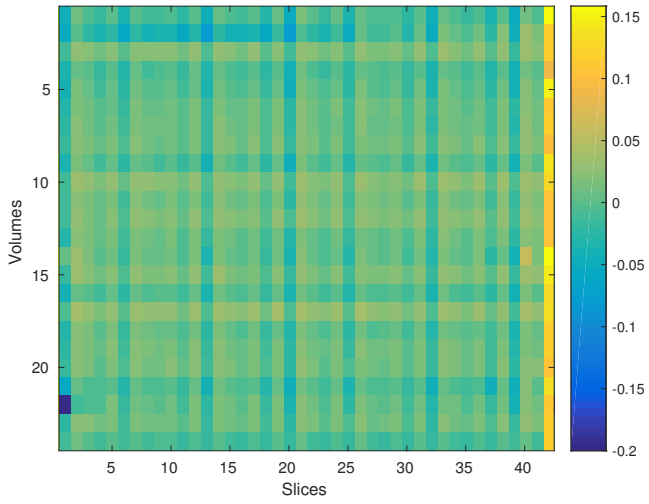

Figure A.16: *Slice-volume representation for the motion estimation of r_y (EPI sequence) using the triggers from the EEG measurement.*

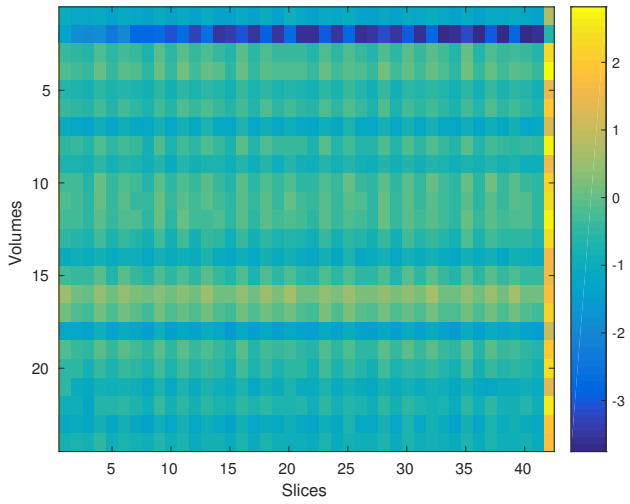

Figure A.17: *Slice-volume representation for the motion estimation of r_z (EPI sequence) using the triggers from the EEG measurement.*

A.2.4 Results when one trigger is used, with subtraction of the regression weights

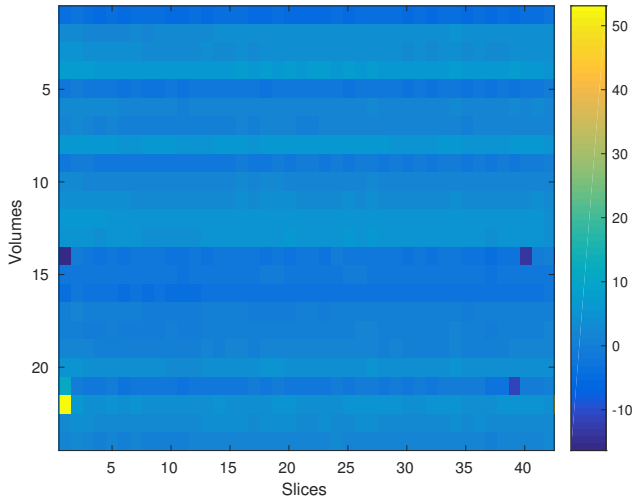

Figure A.18: *Slice-volume representation for the motion estimation of t_x (EPI sequence) using the triggers from the EEG measurement, after the volume subtraction.*

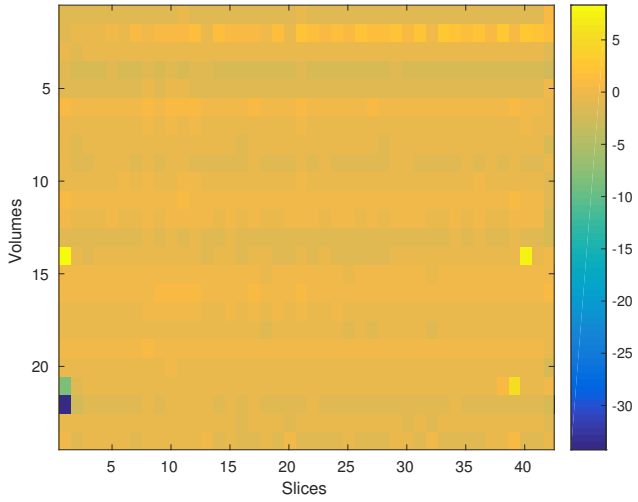

Figure A.19: *Slice-volume representation for the motion estimation of t_y (EPI sequence) using the triggers from the EEG measurement, after the volume subtraction.*

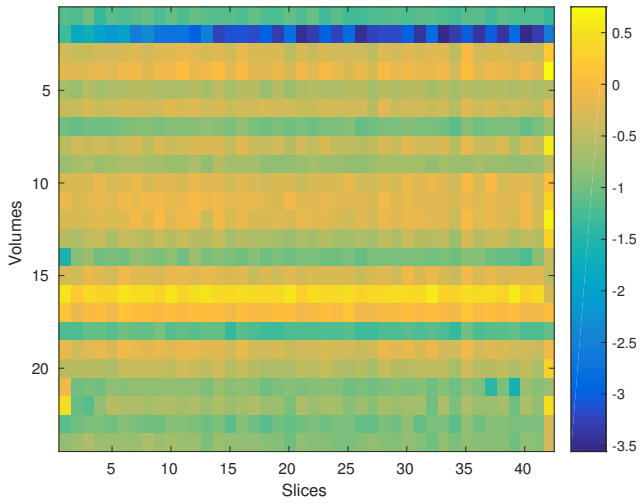

Figure A.20: *Slice-volume representation for the motion estimation of t_z (EPI sequence) using the triggers from the EEG measurement, after the volume subtraction.*

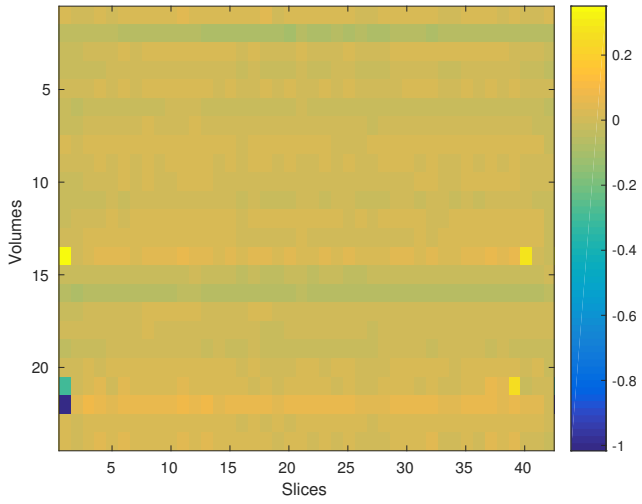

Figure A.21: *Slice-volume representation for the motion estimation of r_y (EPI sequence) using the triggers from the EEG measurement, after the volume subtraction.*

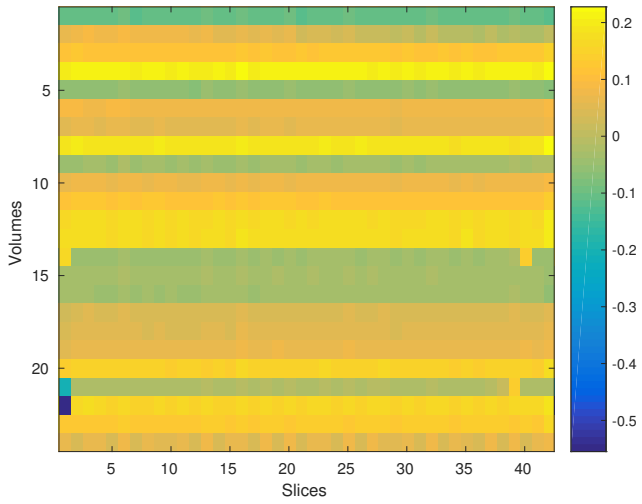

Figure A.22: *Slice-volume representation for the motion estimation of r_z (EPI sequence) using the triggers from the EEG measurement, after the volume subtraction.*

Bibliography

[1] Brainvision recorder user manual. `http://tsgdoc.socsci.ru.nl/images/d/d1/BrainVision_Recorder_UM.pdf`, 2013.

[2] Agamennoni, G., Nieto, J. I., and Nebot, E. M. An outlier-robust kalman filter. In *Robotics and Automation (ICRA), 2011 IEEE International Conference on* (2011), IEEE, pp. 1551–1558.

[3] Allen, P. J., Josephs, O., and Turner, R. A method for removing imaging artifact from continuous eeg recorded during functional mri. *Neuroimage 12*, 2 (2000), 230–239.

[4] Andersen, M. Towards motion-insensitive magnetic resonance imaging using dynamic field measurements.

[5] Chan, S., Zhang, Z., and Tse, K. A new robust kalman filter algorithm under outliers and system uncertainties. In *2005 IEEE International Symposium on Circuits and Systems* (2005), IEEE, pp. 4317–4320.

[6] Chang, L. On kalman-like finite impulse response filters. *arXiv preprint arXiv:1501.07132* (2015).

[7] Cohen, M. S. Echo-planar imaging (epi) and functional mri. *Functional MRI* (1998), 137–148.

[8] Friston, K. J. Introduction. experimental design and statistical parametric mapping. `http://www.fil.ion.ucl.ac.uk/spm/doc/intro/intro.pdf`, 2016.

[9] Garreffa, G., Carni, M., Gualniera, G., Ricci, G., Bozzao, L., De Carli, D., Morasso, P., Pantano, P., Colonnese, C., Roma, V., et al. Real-time mr artifacts filtering during continuous eeg/fmri acquisition. *Magnetic resonance imaging 21*, 10 (2003), 1175–1189.

[10] Hanson, L. G. Introduction to magnetic resonance imaging techniques.

[11] Kalman, R. E. A new approach to linear filtering and prediction problems. *Journal of basic Engineering 82*, 1 (1960), 35–45.

[12] Lobach, V. Kalman filtering algorithm in presence of outliers.

[13] Maclaren, J., Herbst, M., Speck, O., and Zaitsev, M. Prospective motion correction in brain imaging: a review. *Magnetic resonance in medicine 69*, 3 (2013), 621–636.

[14] Maggioni, E., Arrubla, J., Warbrick, T., Dammers, J., Bianchi, A. M., Reni, G., Tosetti, M., Neuner, I., and Shah, N. J. Removal of pulse artefact from eeg data recorded in mr environment at 3t. setting of ica parameters for marking artefactual components: Application to resting-state data. *PloS one 9*, 11 (2014), e112147.

[15] Negishi, M., Abildgaard, M., Nixon, T., and Constable, R. T. Removal of time-varying gradient artifacts from eeg data acquired during continuous fmri. *Clinical neurophysiology 115*, 9 (2004), 2181–2192.

[16] Rorden, C. Slice time correction. `http://www.mccauslandcenter.sc.edu/crnl/tools/stc`, 2016.

[17] Sarkka, S., Vehtari, A., and Lampinen, J. Time series prediction by kalman smoother with cross-validated noise density. In *Neural Networks, 2004. Proceedings. 2004 IEEE International Joint Conference on* (2004), vol. 2, IEEE, pp. 1653–1657.

[18] Smink, J., Häkkinen, M., Holthuizen, R., Krueger, S., Ries, M., Berber, Y., Moonen, C., Köhler, M., and Vahala, E. external control (xtc): a flexible, real-time, low-latency, bi-directional scanner interface. In *Proc Intl Soc Mag Reson Med* (2011), vol. 20, p. 1755.

[19] Thacker, N., and Lacey, A. Tutorial: The kalman filter. *Imaging Science and Biomedical Engineering Division, Medical School, University of Manchester. TiNA* (1998).

[20] Ting, J.-A., Theodorou, E., and Schaal, S. A kalman filter for robust outlier detection. In *2007 IEEE/RSJ International Conference on Intelligent Robots and Systems* (2007), IEEE, pp. 1514–1519.

[21] Vasuhi, S., Vijayakumar, M., and Vaidehi, V. Real time multiple human tracking using kalman filter. In *Signal Processing, Communication and Networking (ICSCN), 2015 3rd International Conference on* (2015), IEEE, pp. 1–6.

[22] Welch, G., and Bishop, G. An introduction to the kalman filter. department of computer science, university of north carolina, 2006.

[23] White, N., Roddey, C., Shankaranarayanan, A., Han, E., Rettmann, D., Santos, J., Kuperman, J., and Dale, A. Promo: Real-time prospective motion correction in mri using image-based tracking. *Magnetic Resonance in Medicine 63*, 1 (2010), 91–105.

[24] Zhao, J., Liu, W.-J., and Sun, H.-J. A motion tracking method based on kalman filter combined with mean-shift. In *2008 International Conference on Wavelet Analysis and Pattern Recognition* (2008), vol. 1, IEEE, pp. 91–95.